© 2018. Published by The Company of Biologists Ltd | Development (2018) 145, dev159566. doi:10.1242/dev.159566

RESEARCH ARTICLE

Cytoplasmic polyadenylation-mediated translational control of maternal mRNAs directs maternal-to-zygotic transition

Cecilia Lanny Winata[1,2,*], Maciej Łapiński[1], Leszek Pryszcz[1], Candida Vaz[3], Muhammad Hisyam bin Ismail[4], Srikanth Nama[4], Hajira Shreen Hajan[5], Serene Gek Ping Lee[5], Vladimir Korzh[1,6], Prabha Sampath[4,7,8], Vivek Tanavde[3,4] and Sinnakaruppan Mathavan[5,9,*]

ABSTRACT

In the earliest stages of animal development following fertilization, maternally deposited mRNAs direct biological processes to the point of zygotic genome activation (ZGA). These maternal mRNAs undergo cytoplasmic polyadenylation (CPA), suggesting translational control of their activation. To elucidate the biological role of CPA during embryogenesis, we performed genome-wide polysome profiling at several stages of zebrafish development. Our analysis revealed a correlation between CPA and polysome-association dynamics, demonstrating a coupling of translation to the CPA of maternal mRNAs. Pan-embryonic CPA inhibition disrupted the maternal-to-zygotic transition (MZT), causing a failure of developmental progression beyond the mid-blastula transition and changes in global gene expression that indicated a failure of ZGA and maternal mRNA clearance. Among the genes that were differentially expressed were those encoding chromatin modifiers and key transcription factors involved in ZGA, including *nanog*, *pou5f3* and *sox19b*, which have distinct CPA dynamics. Our results establish the necessity of CPA for ensuring progression of the MZT. The RNA-seq data generated in this study represent a valuable zebrafish resource for the discovery of novel elements of the early embryonic transcriptome.

KEY WORDS: Cytoplasmic polyadenylation, Translational regulation, Maternal mRNA, Maternal-to-zygotic transition, Zebrafish, Polysome profiling

INTRODUCTION

A period of transcriptional silence follows fertilization in animal embryogenesis, during which development is mainly driven by maternally deposited mRNAs and proteins (Korzh, 2009). At a certain time point, the transition of developmental control from maternal to zygotic occurs (Tadros and Lipshitz, 2009). This event is referred to as the maternal-to-zygotic transition (MZT) and is represented by the occurrence of zygotic genome activation (ZGA; Newport and Kirschner, 1982), the mass degradation of maternal mRNAs (Hamatani et al., 2004; Piko and Clegg, 1982; Walser and Lipshitz, 2011) and major epigenetic reprogramming (Lindeman et al., 2011; Vastenhouw et al., 2010). Transcriptional silence necessitates gene regulation at a different level to ensure appropriate activity of maternal mRNAs. Translational regulation of maternal mRNAs by cytoplasmic polyadenylation (CPA) is crucial for the timely activation of maternal mRNAs during oocyte maturation and the early embryonic development of several model organisms (Aoki et al., 2003; Evsikov et al., 2004; Hwang et al., 1997; Lieberfarb et al., 1996; Oh et al., 2000; Potireddy et al., 2006; Salles et al., 1992). However, there is still a lack of understanding of its biological function and molecular targets during embryogenesis.

In fish and frogs, the mid-blastula transition (MBT) represents a key event within the MZT. At the cellular level, notable changes include the asynchronization of cell division, the acquisition of cell motility and gastrulation (Newport and Kirschner, 1982; Rott and Sheveleva, 1968). The MZT is thus a continuous process that encompasses MBT events, including zygotic genome activation (ZGA), which marks the initiation of gastrulation, together with maternal mRNA clearance. In zebrafish, MBT is initiated at the 10th cell cycle and represents a continuous process lasting approximately until the 13th cell cycle (Kane and Kimmel, 1993). We previously identified a large cohort of maternal mRNAs that undergo CPA during the course of embryogenesis, leading to the MBT in zebrafish (Aanes et al., 2011). Strikingly, CPA occurred almost exclusively prior to the MBT, which led us to question whether these RNAs are implicated in the regulation of this important developmental transition.

Several key elements regulate ZGA. First, maternal inhibiting factors need to be titrated by an increase in DNA content as a result of cell division that increases the nucleocytoplasmic ratio (Dekens et al., 2003; Evsikov et al., 1990; Kane and Kimmel, 1993; Newport and Kirschner, 1982). Concentrated extracts of *Xenopus* eggs contain active transcription machinery, but these are outcompeted by the abundant supply of maternal histones, resulting in the overall repression of transcription (Amodeo et al., 2015; Prioleau et al., 1994). Histones have also been implicated in regulating the accessibility of the genome to activating transcription factors that determine the onset of ZGA (Joseph et al., 2017; Pálfy et al., 2017). In addition to the large supply of histones for chromatin assembly, the bivalent modification of these histone proteins was observed both prior to the MBT and at the MBT in various organisms (Andersen et al., 2013). The nuclear-to-cytoplasmic volume ratio has also been implicated to play a role in determining the timing of ZGA independently of DNA levels (Jevtić and Levy, 2015, 2017). Second, the timely induction of activating factors serves to promote ZGA (Aoki et al., 2003; Oh et al., 2000). In zebrafish, several maternal factors have previously been implicated in this process,

[1]International Institute of Molecular and Cell Biology in Warsaw, 02-109 Warsaw, Poland. [2]Max-Planck Institute for Heart and Lung Research, 61231 Bad Nauheim, Germany. [3]Bioinformatics Institute, Agency for Science Technology and Research, 138671 Singapore. [4]Institute of Medical Biology, Agency of Science Technology and Research, 138648 Singapore. [5]Genome Institute of Singapore, Agency of Science Technology and Research, 138672 Singapore. [6]Institute of Molecular and Cell Biology, Agency of Science Technology and Research, 138673 Singapore. [7]Yong Loo Lin School of Medicine, National University of Singapore, 117596 Singapore. [8]Program in Cancer and Stem Cell Biology, Duke-NUS Medical School, 169857 Singapore. [9]Vision Research Foundation, Sankara Nethralaya, 600 006 Chennai, India.

*Authors for correspondence (cwinata@iimcb.gov.pl; mathavans@gmail.com)

C.L.W., 0000-0002-7718-5248; S.M., 0000-0003-1029-7891

Received 22 September 2017; Accepted 20 November 2017

Development (2018) 145, dev159566. doi:10.1242/dev.159566

namely *nanog*, *pou5f3* and *sox19b* (Lee et al., 2013; Onichtchouk et al., 2010; Xu et al., 2012).

Here, we investigate the association of maternal and early zygotic transcripts with polysomes during the first few hours of embryonic development over the course of the MZT. Our analysis revealed distinct polysome association dynamics of cytoplasmically polyadenylated maternal mRNAs. We found that developmental progression through the MZT depends on the precise translational activation of a subset of maternal mRNAs by CPA. Our data revealed the complexity of mRNA expression dynamics and showed that CPA is essential for two key developmental events that determine embryonic passage through the MZT: (1) ZGA and (2) the clearance of a large number of maternal transcripts.

RESULTS

Transcriptome profiling of polysome fractions and expression clustering

To profile the translational regulatory landscape during early zebrafish development, we performed polysome profiling at several developmental stages: activated unfertilized egg (egg), pre-MBT (1-cell, 16-cell and 128-cell), MBT [high, 3.5 h post-fertilization (hpf)] and post-MBT (50% epiboly, 5.3 hpf). Two fractions that were distinguishable by their density due to the presence or absence of polysome association were isolated and sequenced (Fig. 1A, Fig. S1, Table S1). Unfractionated total RNA from corresponding stages were also sequenced to provide a measure of overall transcript level. Using the total unfractionated RNA-seq dataset, we classified the transcriptome into two broad categories based on their origin: maternal and zygotic. We defined RNAs with transcripts that were present at high (≥10TPM) levels at the egg stage and did not increase before 3.5 hpf as maternal, regardless of whether zygotic contributions exist later on. We defined RNAs that were expressed only from 3.5 hpf onwards as zygotic. We also assigned the pre-MBT cluster to accommodate transcripts whose expression increased prior to 3.5 hpf. Applying these criteria to the RNA-seq data of the total (unfractionated) mRNA, we obtained 9154 maternal genes, 831 pre-MBT genes and 667 zygotic genes (Fig. 1B, Table S2).

To validate our gene clusters, we compared our data with that of Harvey et al. (2013), in which crosses between different zebrafish strains were performed to enable distinctions between maternal and paternal alleles by single-nucleotide polymorphisms (SNPs). To allow direct comparisons, we re-analyzed the raw sequencing reads from this dataset and identified 4393 genes that had both maternal and paternal alleles (maternal-zygotic and zygotic genes) and 487 genes that had only maternal alleles (maternal genes). We found that 337 genes (69%) and 21 genes (4%) out of 487 genes with maternal-only alleles were within our maternal and pre-MBT clusters, respectively, whereas none of these were in the zygotic cluster

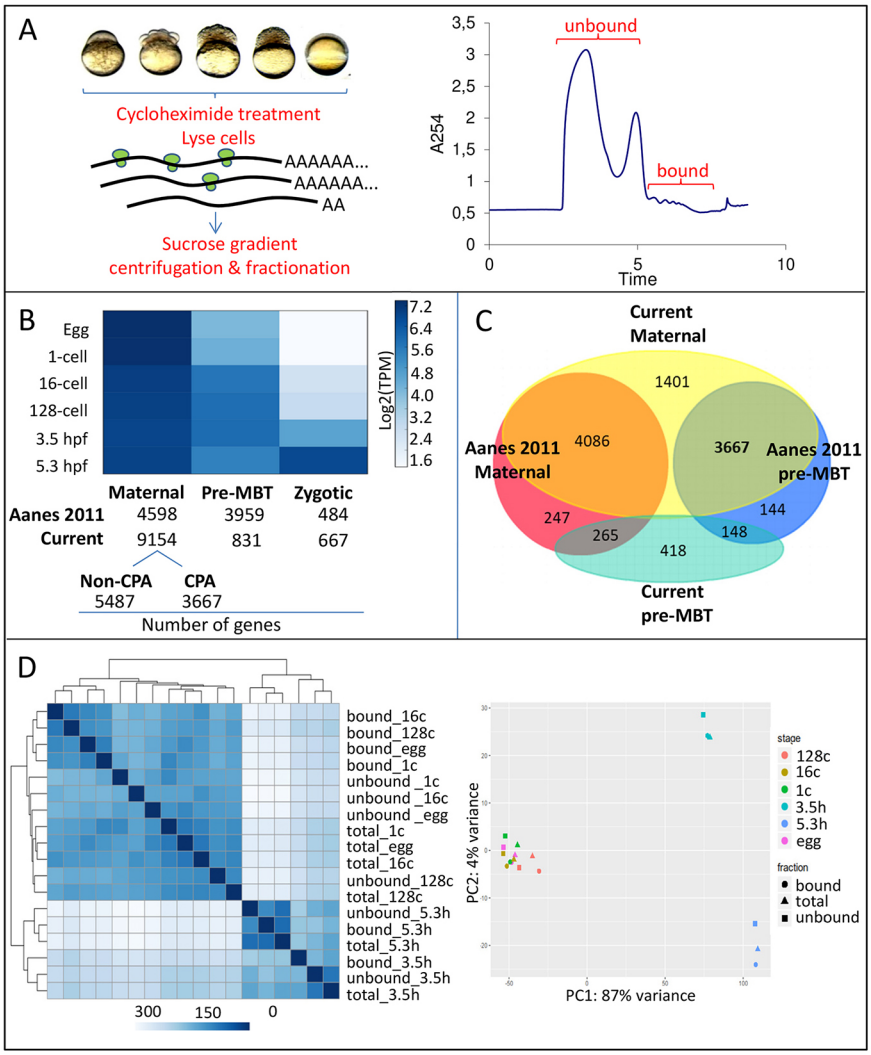

Fig. 1. Polysome profile of the early embryo. (A) Polysome fractionation based on density gradient centrifugation. For each stage, two pooled fractions were obtained that contained polysome-unbound and polysome-bound mRNAs. (B) Gene expression clustering across developmental stages. Genes from Aanes et al. (2011) and the present dataset were clustered into maternal, pre-MBT and zygotic clusters. The maternal cluster was further subdivided based on pre-MBT increase in expression of transcripts that underwent CPA in the Aanes dataset that was attributable to oligo d(T) selection bias. (C) Venn diagram showing overlap between maternal and pre-MBT clusters from both datasets. Notice the large overlap between the Aanes pre-MBT and present maternal cluster. (D) Clustering heat-map and principal component analysis of total and polysome-fractionated samples based on the expression of annotated genes (Ensembl), showing a major division between early and late (MBT and post-MBT) developmental stages. Clustering was performed based on the abundance of transcript level to compute the distances between samples (different color intensity).

Development (2018) 145, dev159566. doi:10.1242/dev.159566

(Table S18). The lack of overlap between the maternal-only genes and our zygotic cluster confirmed the zygotic origin of these genes. A total of 3755 genes (85%), 127 genes (3%) and 41 genes (0.9%) out of 4393 genes that had both maternal and paternal alleles in Harvey et al. (2013) dataset were within the maternal, pre-MBT and zygotic clusters, respectively, reflecting the zygotic contribution for these genes. Altogether, the results of these comparisons suggested that the method used in our study was able to distinguish maternal from zygotic genes.

To assess the association between translational regulation and CPA, identity needs to be assigned to transcripts based on their polyadenylation state. We focused on the maternal group of transcripts to identify those that underwent CPA during pre-MBT stages. As we employed mRNA isolation methods based on rRNA depletion, the information on the lengthening of the poly(A) tail of mRNAs that underwent CPA could not be inferred from this dataset. Therefore, we revisited our previous RNA-seq dataset (Aanes et al., 2011), in which mRNA isolation was performed using oligo d(T) selection that is biased towards those with a longer poly(A) tail. Thus, in the case of transcripts that underwent CPA, this results in an artificial increase in transcript level over time prior to the MBT. This particular group was represented by the 'pre-MBT' cluster in this dataset. We re-analyzed this dataset using the same criteria as those used for the current dataset to determine maternal, pre-MBT and zygotic transcripts, and re-mapped the raw reads to the latest genome assembly (zv10). Re-analysis of this dataset resulted in 3959 pre-MBT, 4598 maternal and 484 zygotic genes (Fig. 1B, Table S2).

We then compared clusters that were derived from the two datasets. The numbers of genes in the zygotic clusters were comparable, but a substantial majority of Aanes pre-MBT transcripts [3667 genes (92.6%)] shifted to the maternal cluster in the rRNA-depleted dataset (Fig. 1C). This observation was consistent with the situation in which these 3667 mRNAs were truly undergoing CPA. Thus, we defined three distinct expression clusters in our current data: a maternal cluster [which was subdivided into a non-cytoplasmically polyadenylated subcluster (non-CPA, 5487 genes, 60%; and a cytoplasmically polyadenylated subcluster (CPA, 3667 genes, 40%)]; a pre-MBT cluster (831 genes); and a zygotic cluster (667 genes).

Among non-CPA subcluster transcripts, GO terms that were enriched (P<0.01) included 'translation', 'DNA repair', 'cell cycle' and 'chromatin modification' (Fig. S3, Table S3). These are relevant to embryonic development prior to the MBT when transcription is absent and embryonic cells undergo synchronous divisions. Interestingly, the enriched categories also included 'mRNA splicing'. Maternal mRNAs are known to be spliced into a mature form prior to embryogenesis, and the presence of transcripts that regulate this process possibly represent a trace of earlier events that preceded fertilization. The CPA subcluster was enriched in several GO terms, including 'protein transport', 'ubiquitin-mediated protein catabolic process' and 'cell cycle' (Fig. S3, Table S4). Interestingly, this cluster also contained notable genes that were implicated in early developmental defects (Abrams and Mullins, 2009). These include *buc* (Dosch et al., 2004), *piwil2* (Houwing et al., 2008), *mapkapk2a* and *chuk* (Wagner et al., 2004), and *dhx16* (Pelegri and Mullins, 2004). In contrast, the zygotic cluster was enriched in GO terms related to embryonic patterning, such as 'cell migration involved in gastrulation', 'dorsal/ventral pattern formation' and 'regulation of endoderm and mesoderm fate specification' (Fig. S3, Table S5). Notably, this cluster was also enriched in transcription factors, likely reflecting the earliest transcriptional activity following ZGA.

Surprisingly, 831 transcripts were identified as being expressed pre-MBT. Libraries were prepared using an rRNA depletion method, and the presence of such transcripts suggests true increase in abundance prior to ZGA. These possibly represent the earliest wave of zygotic transcription that precedes the main wave at MBT. This group was enriched in the GO terms 'nucleosome assembly' and 'chromatin silencing', and contained transcripts encoding nucleosome core components (Fig. S3, Table S6), including multiple histone-encoding transcripts, which are non-polyadenylated (Marzluff, 2005). Our rRNA depletion-based strategy thus enabled their detection as a proof of principle of the improved detection of unique transcripts using this approach. To validate pre-MBT genes as true early zygotic transcripts, we compared them with those that were previously identified as first-wave genes (Lee et al., 2013). The comparison returned a very small overlap (14 of 269 first-wave genes and 831 pre-MBT genes; Table S18). We speculated that this might be caused by the later stage observed in the Lee study (4 hpf, dome stage), such that their gene list would also include zygotic genes that were initiated at the typical timing of ZGA (from 3.5 hpf in the present study). Indeed, a larger overlap (76 genes out of 269 first-wave genes and 667 zygotic genes) was observed with our zygotic cluster genes. Additionally, because our maternal cluster also contained genes with a zygotic contribution (i.e. maternal-zygotic genes), we obtained an equally sizeable overlap (86 genes out of 269 first-wave genes and 9154 maternal genes). Although the differences in the observed stages did not allow the validation of pre-MBT transcripts, it reaffirmed the zygotic origin of those within our zygotic cluster. We then turned to another dataset where early zygotic genes were detected through 4-sUTP labeling of nascent transcripts (Heyn et al., 2014). We found 257 out of the 592 genes reported as early zygotic genes in common with our dataset. However, these genes were distributed between the maternal, pre-MBT and zygotic clusters (113, 53 and 91 genes, respectively). It is worth noting that 440 of the early zygotic genes in Heyn dataset were also maternal-zygotic, some of which would unsurprisingly distribute to our maternal cluster. Additional differences were also caused by their ability to detect many miRNA species (56 in total), which is not the case in our dataset due to different methods used to isolate mRNAs. Owing to the unavailability of other comparable transcriptome data, we could not validate the remainder of the pre-MBT cluster genes. Nevertheless, their robust increase in transcript levels pre-MBT suggests contribution from zygotic transcription to this increase.

Maternal mRNAs that undergo CPA are translationally regulated prior to the MBT

Hierarchical clustering and principal component analysis based on transcriptome profiles revealed tight grouping according to polysome association for samples prior to MBT and according to developmental stage for the MBT and post-MBT samples (Fig. 1D). Although this reflects the relatively constant nature of maternal mRNA composition, the distinction between polysome-bound and -unbound fractions suggests the presence of selective polysome engagement of transcripts prior to MBT. However, this selectivity disappeared at the MBT and post-MBT stages, indicated by the comparatively similar transcriptome profiles of both fractions. This is consistent with the observation that the length of poly(A) tail determined the translation rate only at 2 hpf and not at 4 or 6 hpf (Subtelny et al., 2014). The differential clustering behavior of the samples from the early and late stages thus reaffirms the notion that pan-embryonic translational regulation operates only on maternal mRNAs prior to the MBT.

Development (2018) 145, dev159566. doi:10.1242/dev.159566

To determine whether the CPA of maternal transcripts corresponds to their translational regulation, we performed a stepwise analysis of the polysome-bound and -unbound datasets. First, we sought to determine whether CPA correlates with the recruitment of transcripts to polysomes. We calculated the polysome association of each transcript species as a ratio of bound fraction over the total (bound+unbound) fraction (Fig. 2A). Taking the average values of all of the transcripts in a cluster, a decreasing trend of polysome association was observed in the non-CPA subcluster, whereas an opposite trend indicating an increase in polysome association was observed for the CPA subcluster (Fig. 2A). Next, we defined translational regulation as a disproportionate change in translation compared with transcript level. We reasoned that if translational regulation is exclusive to maternal mRNAs, then an increase in polysome association should be observed only in this subset and not in the subset of zygotic transcripts. We first defined the transcript level (TS) by measure of total mRNA levels and translation (TL) by measure of bound fraction (Fig. 2B). Using the egg stage as a baseline, we calculated the ΔTS and ΔTL of each transcript for each developmental stage. We classified transcripts based on their ΔTS: transcript level up or down (>2-fold compared with egg stage) or constant (<2-fold compared with egg stage). We then defined translational regulation by comparing the ΔTL of each transcript to its ΔTS and classified them as translationally up if ΔTL>ΔTS and translationally down if ΔTL<ΔTS. Thus, we obtained six different combinations of transcript level changes and translational profiles that we applied to transcripts of the non-CPA and CPA subclusters at each developmental stage (Table S7).

At the one-cell stage, the transcriptome consisted mostly of transcripts with constant transcript levels and modest changes in translation (<2-fold). As development proceeded, a decreasing correlation between ΔTS and ΔTL with modest changes in the former and more prominent changes in the latter was observed (Pearson's R=0.63 at the one-cell stage and R=0.21 at the 128-cell stage). This contrasts with what was observed at 5.3 hpf, in which a much larger correlation was found between ΔTS and ΔTL (Pearson's R=0.86). In agreement with the dynamics of the global polysome association (Fig. 2A), the two maternal subclusters had opposing profiles. The CPA subcluster exhibited a shift towards an increase in translation (Pearson's R=−0.005 at the 128-cell stage) and the non-CPA subcluster shifted toward a decrease in translation (Pearson's R=0.036 at the 128-cell stage; Fig. 2C-I). The peak of translational regulation appeared to occur at the 128-cell stage (Fig. 2H,I), in which the correlation between ΔTS and ΔTL was the lowest for both clusters (Fig. 2E). At this stage, the translationally increasing group represented 2464 of 3667 (67%) CPA subcluster transcripts, whereas the translationally decreasing group represented 2972 of 5487 (54%) non-CPA subcluster transcripts (Table S7).

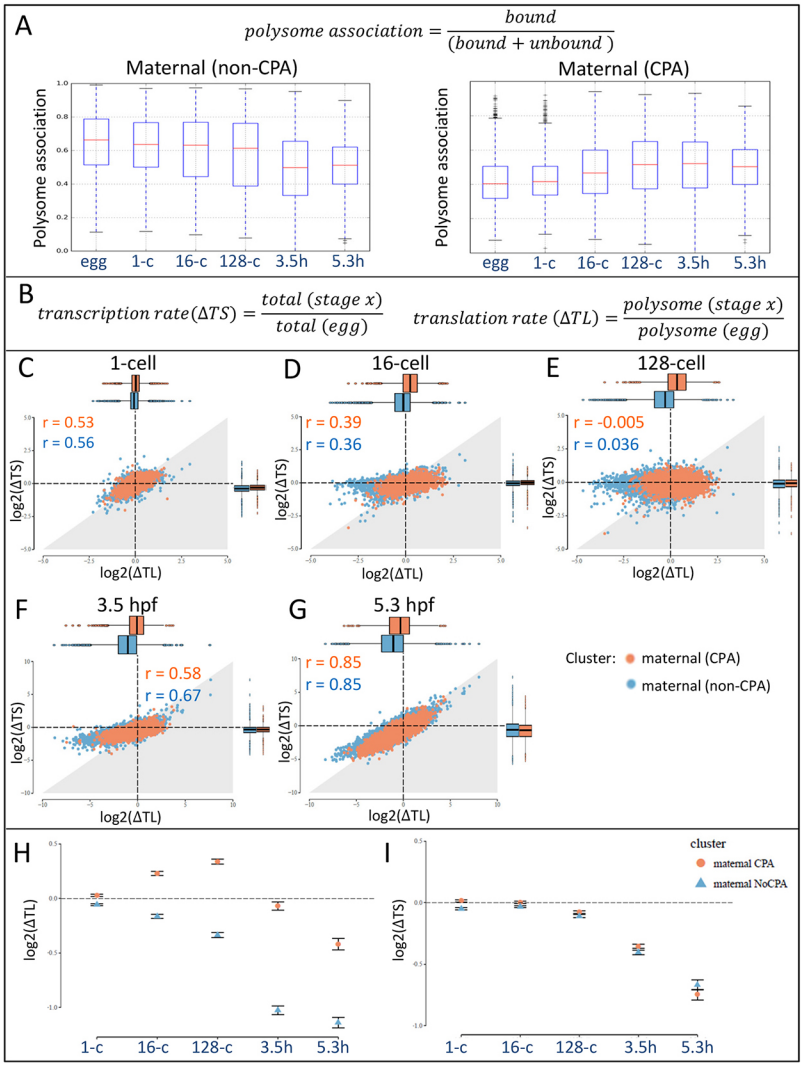

Fig. 2. Polysome association dynamics. (A) Polysome association is expressed as a function of polysome-bound over whole fraction expression values. Distinct dynamics of global polysome association were observed between two maternal subclusters (non-CPA and CPA). (B) Measurements of transcription (ΔTS) and translation (ΔTL) rates were obtained as a fraction of total and polysome-bound expression values at particular stages compared with the egg stage as baseline. Translational regulation is defined as a non-linear relationship between transcription and translation rates. (C-G) Relationship between ΔTS and ΔTL for maternal non-CPA and CPA genes, expressed as a log2 fold change value. Boxplots that represent ΔTS and ΔTL are depicted for the *x*- and *y*-axes, respectively. (H,I) Differential distribution of the median between maternal CPA and non-CPA subclusters in terms of their log2 ΔTL and ΔTS over developmental stages. Significance of the differential distribution was tested using the Wilcoxon two-sample rank-sum test (in all comparisons, P<0.01).

Development (2018) 145, dev159566. doi:10.1242/dev.159566

Interestingly, a considerable number [2079 (38%)] of non-CPA transcripts also translationally increased (Table S7), suggesting that the translation of these transcripts continued during embryogenesis despite their activation in an earlier CPA event prior to fertilization (Oh et al., 2000; Potireddy et al., 2006; Salles et al., 1992). At 3.5 hpf, fewer CPA cluster transcripts [1995 (54%)] were translationally upregulated, possibly reflecting a decline of the previous trend towards an increase in translation, which could be attributable to the initiation of maternal mRNA degradation in this population. Altogether, these observations suggest that maternal mRNAs that undergo CPA also experience positive translational regulation. This was manifested by an increase in the polysome association without a corresponding increase in the level of transcript. Our findings indicated that CPA is a translational regulatory mechanism of maternal transcripts that occurs exclusively during pre-MBT development.

Cytoplasmic polyadenylation is required for gastrulation

To elucidate the biological significance of CPA in embryonic development, we used Cordycepin (3′-dA) to block the polyadenylation of maternal mRNAs. In the embryo, 3′-dA is converted to 3′-dATP, which lacks a 3′-OH group. Thus, its incorporation into the 3′ end of an mRNA molecule inhibits further elongation of its poly(A) tail (Aoki et al., 2003). One of the hallmarks of the MBT is gastrulation, characterized by the initiation of epiboly (Kane and Kimmel, 1993). We previously reported that the inhibition of CPA during pre-MBT development resulted in epiboly arrest and cytolysis of the embryo shortly after MBT [*n*=40; Fig. 3A-G; (Aanes et al., 2011)]. This phenotype was reminiscent of the phenotype of maternal mutants that affected epiboly (Kane et al., 1996; Wagner et al., 2004). To expand our analysis on the role of CPA in the MBT, we performed a shorter pulse of 3′-dA treatment (128-cell to 3.5 hpf). This treatment did not cause developmental arrest, but epiboly was delayed and embryonic patterning was significantly affected (*n*=30; Fig. 3H-K). This suggests that immediately prior to the MBT, development still depends on the CPA of maternal transcripts. Treatment from the one-cell stage up to 16-cell (*n*=40) or 128-cell (*n*=40) stages resulted in epiboly arrest and early mortality that is indistinguishable from that of one-cell to 3.5 hpf treatment, implying that possible effects of the latter treatment on the polyadenylation of zygotic transcripts are minimal to none (Fig. S6D-G).

We hypothesize that the translation of maternal mRNAs that undergo CPA is crucial for MBT. We treated embryos with cycloheximide (CHX) to inhibit translational elongation (Obrig et al., 1971) starting at different stages and ending at 3.5 hpf. CHX treatment starting from the one-cell stage blocked development prior to epiboly. These embryos contained fewer cells of uneven sizes (*n*=20; Fig. 3L), suggesting a failure of cytokinesis. Furthermore, as development proceeded, an acellular space formed between the blastoderm and yolk (Fig. 3M). This phenotype resembled cytokinesis-deficient maternal mutants (Dosch et al., 2004; Pelegri and Mullins, 2004; Yabe et al., 2007). Similarly, treatment that began at the 16-cell stage resulted in embryos with larger blastomeres at 3.5 hpf (*n*=61; Fig. 3N, Fig. S6). At later stages, these embryos remained arrested at the high-oblong stage (Fig. 3O,P). Cycloheximide treatment initiated closer to the MBT (128-cell stage) resulted in epiboly arrest followed by mortality, which resembled 3′-dA-treated embryos (*n*=66; Fig. 3Q-S). All of the CHX treatments caused mortality before 24 hpf. This suggests that similar processes were affected, supporting the hypothesis that the translation of CPA transcripts is necessary for MBT.

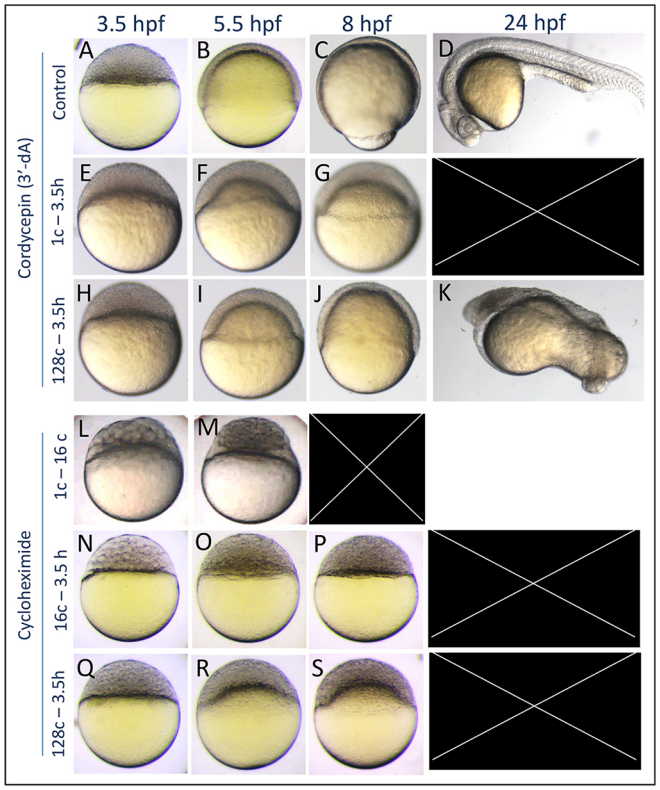

Fig. 3. Epiboly defects caused by 3′dA and CHX treatments. (A-D) Untreated control embryos. (E-G) Embryos that were treated with 3′-dA from the one-cell stage to 3.5 hpf undergo developmental arrest and cytolysis before 24 hpf (*n*=40). (H-K) 3′-dA treatment from the 128-cell stage to 3.5 hpf caused a delay of epiboly and gross patterning defects (*n*=30). (L,M) Translation inhibition by CHX treatment that was initiated at the one-cell stage affected early development and caused early lethality (*n*=20), whereas CHX treatment initiated at the 16-cell stage (N-P) resulted in developmental arrest at the oblong stage (*n*=61). Notice the larger cells at 3.5 hpf, suggesting defects in cell division. (Q-S) Treatment that was initiated at the 128-cell stage resulted in epiboly arrest followed by mortality (*n*=66).

To characterize the phenotype resulting from 3′-dA treatment (one-cell stage to 3.5 hpf) in more detail, we looked at structures that indicate the progression of gastrulation. The yolk syncytial layer (YSL) is formed immediately before gastrulation (Kimmel and Law, 1985). The membrane of the YSL nuclei at the outermost periphery of the embryo [external YSL (e-YSL)] is connected to the overlying blastomeres by tight junctions (Betchaku and Trinkaus, 1978; Solnica-Krezel and Driever, 1994) and provides the driving force for epiboly (Behrndt et al., 2012). The e-YSL nuclei were clearly formed in 3′-dA-treated embryos at 3.5 hpf (*n*=5; Fig. 4A,D), but they were not visible at 5.3 hpf (*n*=5; Fig. 4B,E). Based on the expression of the YSL marker *camsap2a2* at 6 and 8 hpf, the e-YSL was absent, although a weak signal from the inner YSL was still present (*n*=8; Fig. 4G-J). This suggests a delay in the progression of the deep cells compared with the overlying blastomeres. Therefore, 3′-dA treatment inhibited the progression of epiboly.

By 8 hpf, 3′-dA-treated embryos exhibited developmental arrest (Fig. 4C,F) and underwent cytolysis between 9 and 10 hpf. To determine the extent to which gastrulation proceeded in these embryos, we searched for the presence of dorsal shield (i.e. one of the earliest structures formed at gastrulation). In 3′-dA-treated embryos, no defined structure resembling the dorsal shield was observed, and the expression of the dorsal mesoderm marker

Development (2018) 145, dev159566. doi:10.1242/dev.159566

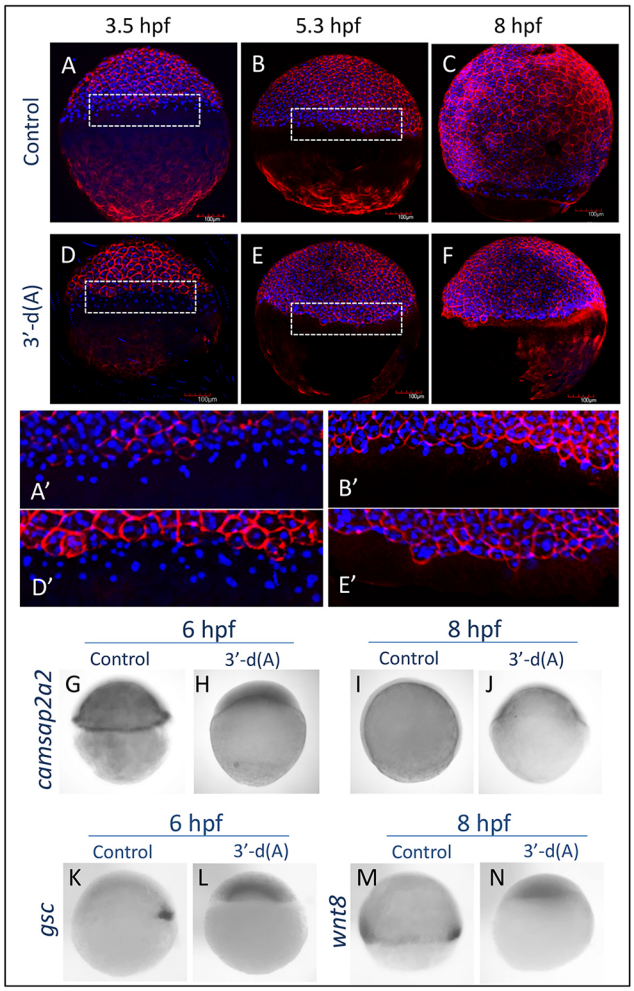

Fig. 4. Phenotype caused by CPA inhibition. (A-C) At 3.5 and 5.3 hpf, the external yolk syncytial layer (e-YSL) could be observed in control embryos. (D-F) Embryos treated with 3′-dA beginning at the one-cell stage to 3.5 hpf still had visible e-YSL at 3.5 hpf, but this structure disappeared by 5.3 hpf, and epiboly did not proceed further (n=5). (G-J) Whole-mount *in situ* hybridization with the YSL marker *camsap2a2* confirmed the absence of e-YSL up to 8 hpf (n=8). Other gastrulation markers, including dorsal shield (K-L; n=8) and mesendodermal cells expressing *wnt8* (M,N; n=8), were also absent.

(prechordal plate) *goosecoid* (*gsc*) was abnormal (n=8; Fig. 4K,L). Furthermore, the expression of *wnt8a*, which defines the ventrolateral mesoderm (Baker et al., 2010), was absent in 3′-dA-treated embryos (n=8; Fig. 4M,N). Together with the absence of the dorsal organizer, this suggests the lack of dorsoventral patterning and ventral mesoderm specification. Collectively, our findings showed that inhibition of CPA by 3′-dA resulted in a failure of developmental progression through the MBT, indicated by the absence of early hallmarks of gastrulation.

Cytoplasmic polyadenylation inhibition affects zygotic genome activation and maternal mRNA clearance

To elucidate the molecular events that underlie the control of MZT by CPA, we performed gene expression analysis using microarrays. We inhibited CPA by 3′-dA beginning at the one-cell stage until 3.5 hpf (long exposure), from the 16-cell stage until 3.5 hpf (medium exposure) and from the 128-cell stage until 3.5 hpf (short exposure), and assayed changes in gene expression profiles at 3.5 hpf. We identified genes that were consistently regulated (either upregulated or downregulated) in all three treatments because these are considered the most sensitive to 3′-dA treatment. This analysis consisted of a total of 3082 genes (2106 upregulated genes and 976 downregulated genes; P<0.05, fc≥2 in at least one treatment; Table S8). The downregulated group contained a large number of genes encoding transcription factors and were significantly enriched in GO terms related to transcription regulation, dorsoventral pattern formation (e.g. *nog1*, *chd*, *gsc*, *ndr1*, *ndr2* and *bambia*), cell migration in gastrulation [e.g. *mxtx2*, *apela*, *aplnra*, *cxcr4a*, *bon* (*mixl1*) and *rock2a*] and germ layer formation [e.g. *gata5*, *bon*, *wnt11*, *sox32*, *tbx16*, *ntla* (*ta*), *bmp2b*, *vent* and *oep* (*tdgf1*); Table S9]. The downregulation of these functions agrees with the failure of gastrulation that was observed as a result of 3′-dA treatment.

Genes that were upregulated by 3′-dA were enriched in GO terms for DNA repair and chromatin modification, and included several components of chromatin and suppressive chromatin modifiers, such as *ehmt2*, *hdac9b*, *hdac3*, *hdac4*, *setdb1a* and *smarcb1a* (Table S10). The upregulation of these suppressive factors suggests a failure of their clearance. In order to confirm this, we looked at two degradation mechanisms for maternal mRNA clearance that were identified in zebrafish (Giraldez et al., 2006; Zhao et al., 2017). To identify possible interactions between CPA and these two degradation mechanisms, we searched for targets of each of these two degradation pathways among the genes that were affected by CPA inhibition. The targets of zygotically expressed miR-430 were identified as transcripts that were upregulated in MZdicer mutants and had the recognition sequence for miR-430 (Giraldez et al., 2006). Ythdf2, which is maternally expressed, recognizes the N^6-methyladenosine (m^6A) modification of RNAs that mediates their decay. Targets of this pathway were identified as those mRNAs that increased their stability in response to Ythdf2 loss of function (Zhao et al., 2017). We identified 580 genes in common between 3′-dA-upregulated genes and Ythdf2 targets; 33 of these were also targets of miR-430. Additionally, 25 genes upregulated by 3′-dA were miR-430 targets, although they were not Ythdf2 targets (Table S11). This observation supports the role of CPA in maternal mRNA clearance by both maternal and zygotic modes of degradation. Nevertheless, other degradation mechanisms also exist in the zebrafish (Bazzini et al., 2016), which may account for the rest of the maternal transcripts.

We then determined the expression cluster to which the 3′-dA-responsive genes belonged by intersecting them with the total RNA-seq clusters (Fig. 5A). A total of 1457 genes were in common between the two datasets. Among these, a large number of genes that were upregulated by 3′-dA were maternal [1090 out of 1140 (96%)], whereas very few genes were of zygotic origin [50 out of 1140 (4%)]. A total of 174 of the downregulated genes (55%) were of zygotic origin (zygotic and pre-MBT clusters) and 143 (45%) were maternal. Among the downregulated maternal genes, 83 of 143 (58%) had a zygotic contribution, as evidenced by the increase in their transcript level at 3.5 or 5.3 hpf in RNA-seq data. Therefore, the downregulation of these maternal-group genes may reflect failure of the activation of their zygotic counterpart. These observations are consistent with the scenario in which there is a concurrent failure of maternal transcript degradation and zygotic transcription initiation. Downregulated zygotic genes were enriched in similar GO terms to those of the overall microarray set of downregulated genes (Table S12), reflecting the earliest biological functions activated at the MBT, which includes gastrulation, cell fate commitment, convergent extension and the development of different germ layers. These interconnected processes are depicted

Development (2018) 145, dev159566. doi:10.1242/dev.159566

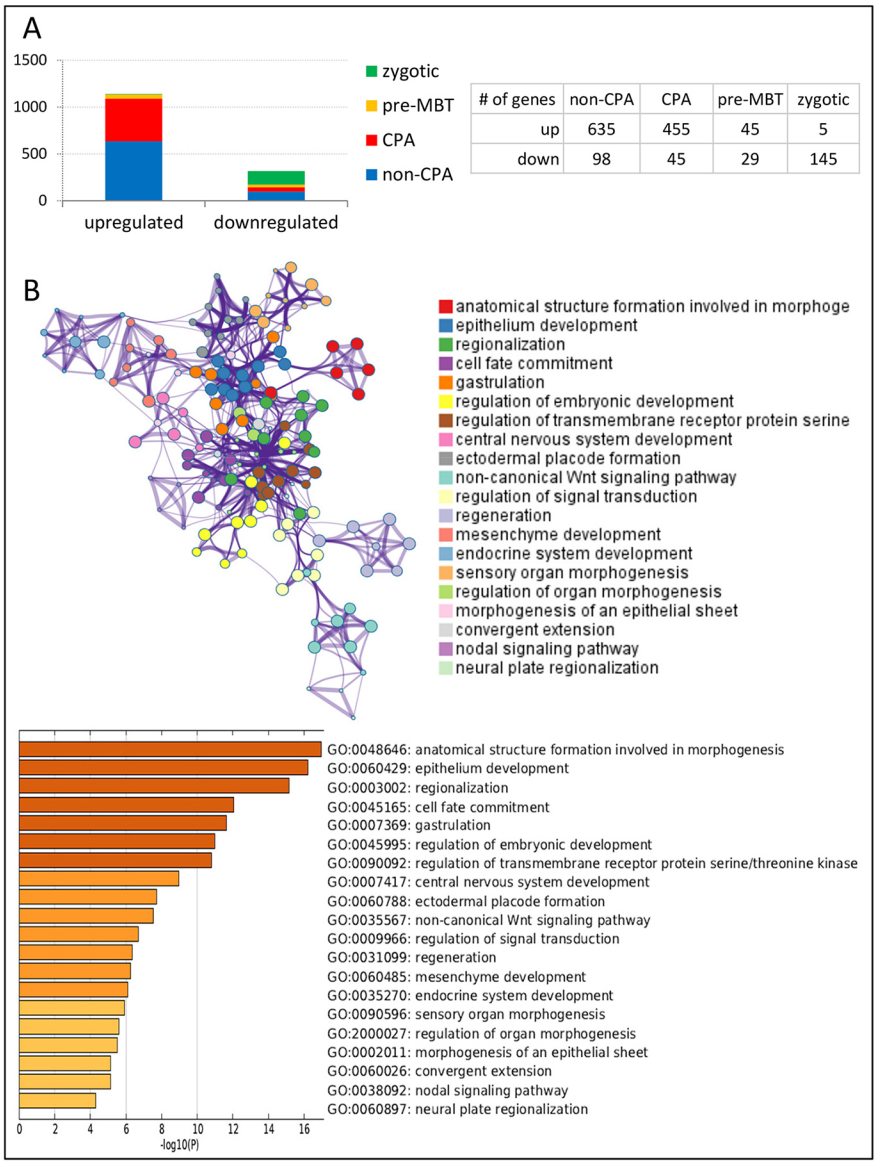

# of genes	non-CPA	CPA	pre-MBT	zygotic
up	635	455	45	5
down	98	45	29	145

Fig. 5. Gene expression changes as a result of 3′-dA treatment. (A) Microarray expression analysis of 3′-dA-treated embryos at 3.5 hpf revealed genes that were responsive to CPA inhibition. Statistically significant gene expression was determined by ANOVA, and threshold values were set as $P<0.05$ and fold-change ≥2. The chart shows the distribution of these 3′-dA-responsive genes in the four expression clusters and subclusters. (B) Enriched biological process terms within 3′-dA-downregulated genes depicted as an interaction network and list according to *P* values. Functions that are related to gastrulation and embryonic development were prominently enriched.

in a network that shows the interactions between different functions (Fig. 5B).

Interestingly, several members of the core histone family, especially from the H2A family, were found among the downregulated pre-MBT genes (Table S13). Upregulated non-CPA genes presented similar GO term enrichment as the overall set of upregulated genes, including suppressive chromatin modifiers (Table S14). The observation of upregulated genes of maternal origin likely resulted from a failure of the transcriptional activation of maternal mRNA degradation components. To a lesser extent, some genes of maternal origin were downregulated as a result of CPA inhibition. These included *pou5f3*, a maternal (non-CPA) transcription factor implicated in ZGA (Lee et al., 2014). Upregulated CPA subcluster genes did not exhibit enrichment of any functional categories. Nonetheless, this group included a notable number of genes involved in protein degradation, including several ubiquitin ligases and their associated components (Table S15).

Altogether, our analyses indicated that the timely activation of maternal mRNA translation by CPA underlies major events associated with the MZT, namely the activation of expression of key zygotic genes that are required for gastrulation and germ layer formation, the degradation of maternal mRNAs and epigenetic adjustments to allow transcriptional activation.

Discovery of novel transcripts in the early embryonic transcriptome

Although more than 95% of the zebrafish genome has been assembled, its annotation is far from complete. A large fraction of our RNA-seq reads mapped to regions outside of those annotated as coding or noncoding transcripts (Fig. S5). We identified a total of 2176 novel transcribed fragments (transfrags), representing 1080 unique genomic loci based on combined RNA-seq reads across all samples. These possessed identifiable ORF characteristics that were at least 100 amino acids long. A considerable fraction exhibited junction-spanning reads, forming multi-exonic transcripts. To validate and annotate the novel identified loci, peptide sequences originating from the longest transfrags of each locus were aligned to the UniRef90 protein database to search for sequence homology to existing annotated transcripts. We identified 1922 transfrags (88%) that originated from 896 genomic loci (83%) (E-value threshold 1e-5).

Development (2018) 145, dev159566. doi:10.1242/dev.159566

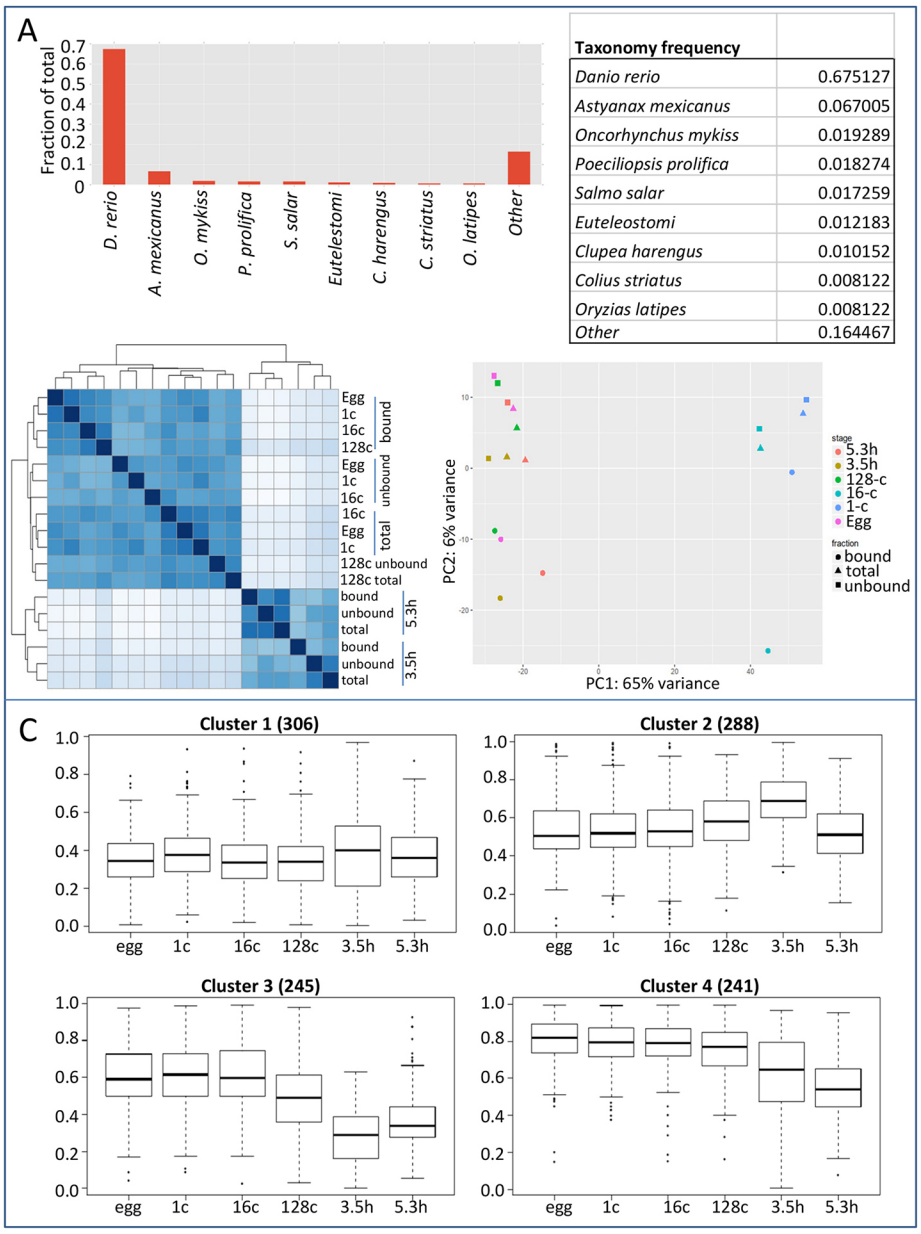

Fig. 6. Discovery of novel transcribed regions in the zebrafish genome. (A) BLAST alignment (E-value threshold=1e-5) revealed that a large majority (88%) of the identified novel transfrags had the highest scoring match to a zebrafish annotated transcript, whereas the others matched annotated transcripts of other fish species. (B) Hierarchical clustering and principal component analysis of novel transfrags revealed similar clustering patterns compared with the annotated genes. (C) Expression clustering of novel transfrags based on translated fractions revealed expression trends that were similar to the annotated transcripts, suggesting their biological significance. Box and whisker plots depicts the distribution of the translated fraction, with the median value indicated by a bold line.

Taking the highest scoring match of each alignment, this corresponded to 878 unique UniRef90 entries, among which 570 were described as 'predicted' and 260 were described as 'uncharacterized' transcripts. Taxonomically, these homologous entries originated from 95 different species, the most prominent of which was *Danio rerio* (67.5%; Fig. 6A). In a parallel analysis, 1566 transfrags (72%) that originated from 770 loci (71%) corresponded to 1977 unique Pfam entries. Among these, the C2H2-type zinc-finger domain was the most prevalent (Fig. S4). Of these novel loci, we further identified 1952 transfrags (89.7%) that had at least one EST support. Altogether, a total of 2021 novel transfrags, representing 971 genomic loci, were annotated. Among these, 1740 transfrags (86%) and 782 genomic loci (80.5%) had both Uniref and EST support (Tables S16 and S17). To assess whether these novel transcripts had an expression profile distribution that was similar to the set of annotated transcripts, we calculated the total normalized read counts for novel genomic loci in each sample and performed clustering analysis. To our surprise, the clustering performed using only the set of novel transcripts presented an almost identical pattern to that of the annotated genes (Fig. 6B). The novel transcripts could also be clustered based on their expression pattern into maternal, pre-MBT and zygotic clusters, thus supporting their authenticity and biological relevance (Fig. 6C).

The high number of novel transfrags that possessed considerable sequence homology to known proteins and recognizable protein domains suggested that they were likely to be authentic and did not result from sample contamination. This also revealed that a considerable number of transcripts were missing from the current annotation, despite having EST support. One likely possibility is that these novel transcripts contain repetitive sequences that caused them to be filtered out during the data analysis. Therefore, our findings reiterate the need for a refinement of analytical strategies to increase the sensitivity of transcript identification. The discovery of novel transcripts would contribute to improving zebrafish genome annotation. More importantly, our datasets were generated without

Development (2018) 145, dev159566. doi:10.1242/dev.159566

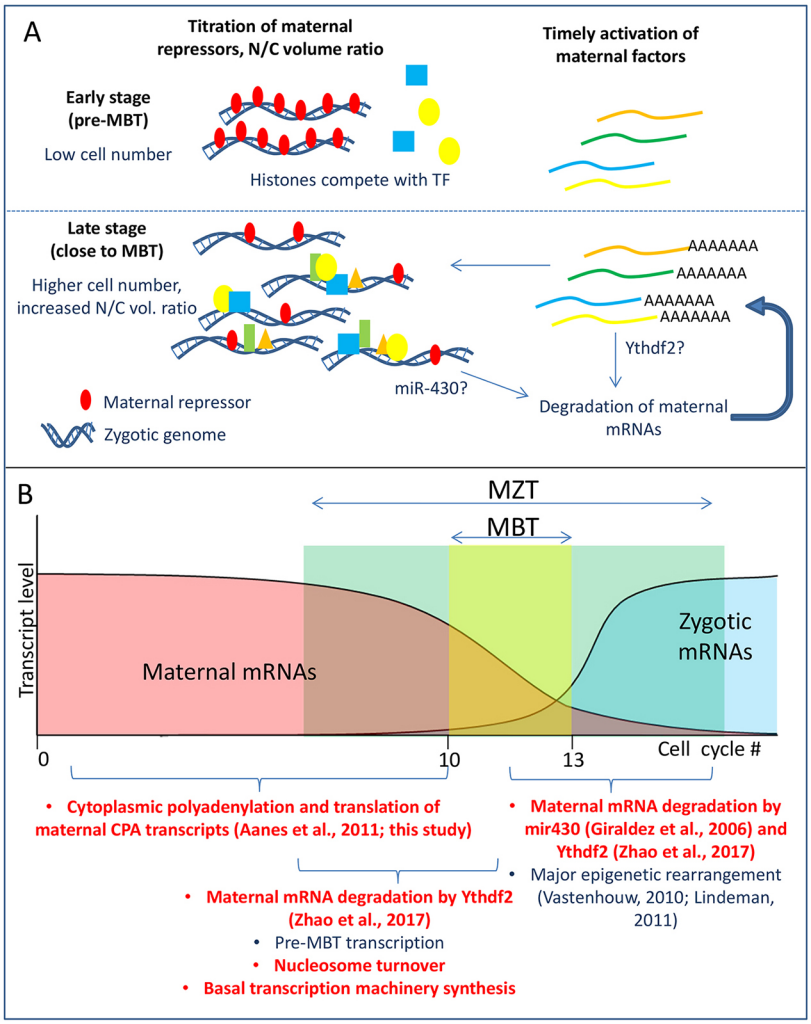

Fig. 7. Proposed model for the role of CPA in regulating MZT. (A) Model of activation of the zygotic genome during the MBT. Maternal repressors that prevent zygotic transcription are present in the early stages following fertilization (red ovals). As cells divide, genomic DNA copy increases, titrating out the repressors and possibly creating access to the genome. Consequently, nuclear-to-cytoplasmic volume ratio increases prior to ZGA. At the same time, a subset of maternal mRNAs are activated through CPA, allowing the synthesis of factors that are required for the activation of transcription (colored shapes) and maternal mRNA clearance. (B) Developmental processes associated with MZT progression. The CPA of maternal mRNAs regulates the timely activation of maternal factors that drive the processes presented in red.

poly(A) tail bias, which enables the accurate detection of transcript levels, particularly in the case of maternal transcripts that are subjected to CPA at pre-MBT stages of development.

DISCUSSION

The polysome association analysis of the early embryonic transcriptome showed that maternal mRNAs that underwent CPA were increasingly associated with polysomes during pre-MBT stages, and their translation increased despite the lack of transcriptional input. One caveat of this analysis was that detection of the polyadenylation state relied on oligo d(T) selectivity based on the increasing length of the poly(A) tail. To define the occurrence of CPA with high confidence, we employed two strategies. First, we imposed a strict differential expression cutoff (see supplementary Materials and Methods) to define the increase in detected transcripts between two consecutive stages. Second, we cross-validated the oligo d(T)-generated dataset with another dataset from identical developmental stages that was generated without poly(A) bias. These strategies allowed us to obtain a robust gene set that could be directly validated by means of several methods (see Aanes et al., 2011) (Fig. S2).

Although translational activation through CPA is known to play an important role in oogenesis (Oh et al., 2000; Potireddy et al., 2006; Salles et al., 1994), its role in embryogenesis has been less appreciated, especially within the context of the MZT. We found that the CPA of a large cohort of maternal mRNAs was essential for the MZT in zebrafish. Cytoplasmic polyadenylation may regulate the MZT in at least two possible ways. First, it facilitates ZGA. Second, it is required for the activation of maternal mRNA degradation. Supporting the first mechanism, many zygotic genes were downregulated in response to pan-embryonic CPA inhibition, implying a failure of their transcriptional activation upon ZGA. Concurrently, upon CPA inhibition, many maternal mRNAs were upregulated, including targets of the two known maternal mRNA degradation mechanisms (Giraldez et al., 2006; Zhao et al., 2017). Defects in maternal mRNA clearance have been shown to affect early developmental events, including those that are associated with the MZT (Yartseva and Giraldez, 2015). Interestingly, Ythdf2 (Zhao et al., 2017) is cytoplasmically polyadenylated during pre-MBT stages, suggesting that its proper function in maternal mRNA degradation relies on translational regulation by CPA. Additionally, miR-430 is expressed zygotically, the activation of which likely depends on CPA. Therefore, one possibility is that CPA regulates the MZT, at least partially by ensuring the clearance of maternal mRNAs by these two degradation pathways.

Among the maternal factors that are known to play a role in zebrafish ZGA (Lee et al., 2013; Onichtchouk et al., 2010; Xu et al., 2012), *nanog* and *pou5f3* were not subjected to CPA during embryonic development. However, *sox19b* falls within the CPA subcluster. Moreover, it exhibited a high degree of translational

Development (2018) 145, dev159566. doi:10.1242/dev.159566

activation by the 128-cell stage, strongly suggesting that *sox19b* is under positive translational regulation during pre-MBT development. Based on loss-of-function analysis of these three factors, a combination of factors rather than the individual action of their activities likely contributes to ZGA (Lee et al., 2013). The stoichiometry between Sox2 and Oct4 (i.e. orthologs of Sox19b and Pou5f3, respectively) is known to affect the reprogramming of somatic cells into induced pluripotent stem cells (Carey et al., 2011; Papapetrou et al., 2009). Moreover, *nanog*, *pou5f3* and *sox19b*, which are well known to be regulators of pluripotency, physically interact with each other, and the dynamics of their interactions correspond to the progression of cell differentiation (Perez-Camps et al., 2016; Rizzino, 2013). Whether the increase in Sox19b translation during development represents a similar mechanism for combinatorial activation of these factors in ZGA remains to be experimentally proven.

Altogether, our findings complement the currently accepted models of ZGA mechanisms by demonstrating a temporal component, in which CPA activates a subset of maternal mRNAs that are required for the MZT (Fig. 7A). Cytoplasmic polyadenylation might be considered an essential part of the mechanism that drives the MZT, which would expand the definition of MZT to encompass all processes that are essential for the transition of developmental control from maternal to zygotic. These would include the CPA of maternal mRNAs and other associated functions that are activated by this mechanism as a part of the MZT in addition to ZGA and maternal mRNA clearance (Fig. 7B).

Proteomics of the zebrafish egg and early embryo still poses technical challenge due to the lack of sensitive techniques and the presence of high molecular weight proteins in the yolk. Thus, there is insufficient knowledge of the factors that are provided maternally as fully functional proteins that might additionally contribute to the regulation of early embryogenesis. Polysome profiles that were identified in the present study provide crucial information on proteins that are synthesized from maternal factors that are deposited as mRNAs. Additionally, the identified novel transcripts are a valuable source of candidate regulators, the detailed functional analysis of which is currently under way. Complementing these data with knowledge of the maternal proteome that shapes the egg and early embryo is a next step towards a more comprehensive understanding of the control of the MZT.

MATERIALS AND METHODS

Zebrafish

Wild-type (AB) zebrafish were maintained in the IMCB zebrafish facility, Singapore. All animal experiments were performed according to the regulations of the Institutional Animal Care and Use Committee (Biological Resource Center, Biopolis). Embryos were maintained and staged according to standard protocols (Kimmel et al., 1995; Westerfield, 2000).

Polysome fractionation

Embryos were collected at one-cell (0 hpf), 16-cell (1.5 hpf), 128-cell (2.5 hpf), high (3.5 hpf) and 50% epiboly (5.3 hpf) stages. Unfertilized eggs were harvested by squeezing the abdomens of spawning female zebrafish. Three hundred eggs or embryos from each stage were immersed in embryo medium containing 200 µg/ml cycloheximide for 10 min, followed by lysis in 500 µl lysis buffer (Sampath et al., 2011). The first four polysome fractions that were pooled as 'polysome-unbound' and the subsequent four polysome fractions that were pooled as 'polysome-bound' were precipitated with 2.5 ml of 100% ethanol for RNA isolation. Validation of expression dynamics in fractionated samples was performed by quantitative reverse transcription polymerase chain reaction (qRT-PCR) of representative genes in polysome-bound and -unbound fractions (Fig. S2).

RNA-seq

RNA was isolated using RNEasy mini kit (Qiagen) with two additional rounds of column-washing steps. Total RNA was rRNA-depleted using Ribo-Zero Magnetic Gold Kit (Human, Mouse, Rat; Epicenter) and quantified using Qubit (Life Technologies). Its quality was assayed using RNA 6000 Nano chip on Agilent 2100 Bioanalyzer. Stranded RNA-seq libraries were generated using ScriptSeq v2 RNA Library Preparation Kit (Illumina) and sequenced on Illumina HiSeq2500 for 75 cycles to a depth of 100 million reads per sample. For detailed bioinformatics analysis methods and discovery of novel transcripts, see supplementary Materials and Methods.

Microarray

Gene expression profiling was performed on a custom zebrafish array (Agilent Technologies, GIS V2) as previously described (Winata et al., 2013). Data analysis was performed in Genespring (Agilent Technologies). The statistical significance of changes in gene expression was determined using one-way analysis of variance (ANOVA); threshold values were set as $P<0.05$ and fold-change ≥ 2. Genes were annotated using BioMart (Smedley et al., 2009).

Chemical treatment

3′-dA treatment was performed as previously described (Aanes et al., 2011). Briefly, embryos were placed in glass Petri dishes containing 4 mM 3′-dA (Sigma-Aldrich, C3394) dissolved in embryo medium. Cyclohexamide treatment was performed with 20 µg/ml cyclohexamide (ROTH, 8682.3) in dimethylsulfoxide (DMSO). The control for CHX treatment was the corresponding amount of DMSO (0.04%) in embryo medium. To terminate the treatment, embryos were rinsed four times with embryo medium and transferred to a new dish containing fresh egg water. Observations were made of at least three independent experiments.

Immunofluorescent staining and confocal microscopy

Immunofluorescent staining was performed according to established protocols (Chu et al., 2012). Confocal imaging was performed using an Olympus FluoView FV1000 (Olympus, Japan). Immunofluorescently labeled embryos were mounted in 0.5% low-temperature melting agarose in embryo medium. Two- or three-dimensional reconstructions of imaging data were performed using the standard Olympus software package.

Whole-mount *in situ* hybridization

Whole-mount *in situ* hybridization was performed as described previously (Winata et al., 2013). Digoxigenin-labeled RNA antisense probes were synthesized from partial cDNA clones of *gsc*, *wnt8a* and *camsap2a2* (details are in the supplementary Materials and Methods), using DIG RNA labeling mix (Roche, Switzerland) and SP6 or T7 polymerase enzyme (Fermentas, Lithuania). Images were captured with a Leica M205FA camera and Zeiss AxioImager.M2.

Acknowledgements

We thank D. Solter, B. Knowles, W. Rybski, L. T. Chu and S. Fong for insightful discussions and technical assistance.

Competing interests

The authors declare no competing or financial interests.

Author contributions

Conceptualization: C.L.W., V.T., S.M.; Methodology: C.L.W., C.V., M.H.b.I., P.S., V.T., S.M.; Validation: C.L.W.; Formal analysis: C.L.W., M.Ł., L.P., C.V., V.T.; Investigation: C.L.W., M.Ł., M.H.b.I., S.N., H.S.H., S.G.P.L.; Data curation: M.Ł., L.P.; Writing - original draft: C.L.W., M.Ł., L.P., V.K., P.S., S.M.; Writing - review & editing: C.L.W., M.Ł., L.P., V.K., P.S.; Supervision: C.L.W., P.S., V.T., S.M.; Project administration: C.L.W., S.M.; Funding acquisition: C.L.W., S.M.

Funding

This work was supported by funding from the Agency for Science, Technology and Research (A*STAR) and the Biomedical Research Council, Singapore. C.L.W. and L.P. are supported by the European Union Seventh Framework Programme (Fishmed GA 316125). M.Ł. is supported by the Narodowe Centrum Nauki (NCN) (OPUS grant 2014/13/B/NZ2/03863) and by a DIAMENTOWY scholarship from the Minister Nauki i Szkolnictwa Wyższego.

Data availability

All sequencing data have been deposited in the GEO database under accession number GSE88776.

Supplementary information

Supplementary information available online at
http://dev.biologists.org/lookup/doi/10.1242/dev.159566.supplemental

References

Aanes, H., Winata, C. L., Lin, C. H., Chen, J. P., Srinivasan, K. G., Lee, S. G. P., Lim, A. Y. M., Hajan, H. S., Collas, P., Bourque, G. et al. (2011). Zebrafish mRNA sequencing deciphers novelties in transcriptome dynamics during maternal to zygotic transition. *Genome Res.* **21**, 1328-1338.

Abrams, E. W. and Mullins, M. C. (2009). Early zebrafish development: it's in the maternal genes. *Curr. Opin. Genet. Dev.* **19**, 396-403.

Amodeo, A. A., Jukam, D., Straight, A. F. and Skotheim, J. M. (2015). Histone titration against the genome sets the DNA-to-cytoplasm threshold for the Xenopus midblastula transition. *Proc. Natl. Acad. Sci. USA* **112**, E1086-E1095.

Andersen, I. S., Lindeman, L. C., Reiner, A. H., Østrup, O., Aanes, H., Alestrom, P. and Collas, P. (2013). Epigenetic marking of the zebrafish developmental program. *Curr. Top. Dev. Biol.* **104**, 85-112.

Aoki, F., Hara, K. T. and Schultz, R. M. (2003). Acquisition of transcriptional competence in the 1-cell mouse embryo: requirement for recruitment of maternal mRNAs. *Mol. Reprod. Dev.* **64**, 270-274.

Baker, K. D., Ramel, M.-C. and Lekven, A. C. (2010). A direct role for Wnt8 in ventrolateral mesoderm patterning. *Dev.Dyn.* **239**, 2828-2836.

Bazzini, A. A., Del Viso, F., Moreno-Mateos, M. A., Johnstone, T. G., Vejnar, C. E., Qin, Y., Yao, J., Khokha, M. K. and Giraldez, A. J., (2016). Codon identity regulates mRNA stability and translation efficiency during the maternal-to-zygotic transition. *EMBO J.* **35**, 2087-2103.

Behrndt, M., Salbreux, G., Campinho, P., Hauschild, R., Oswald, F., Roensch, J., Grill, S. W. and Heisenberg, C.-P. (2012). Forces driving epithelial spreading in zebrafish gastrulation. *Science* **338**, 257-260.

Betchaku, T. and Trinkaus, J. P. (1978). Contact relations, surface activity, and cortical microfilaments of marginal cells of the enveloping layer and of the yolk syncytial and yolk cytoplasmic layers of fundulus before and during epiboly. *J. Exp. Zool.* **206**, 381-426.

Carey, B. W., Markoulaki, S., Hanna, J. H., Faddah, D. A., Buganim, Y., Kim, J., Ganz, K., Steine, E. J., Cassady, J. P., Creyghton, M. P. et al. (2011). Reprogramming factor stoichiometry influences the epigenetic state and biological properties of induced pluripotent stem cells. *Cell Stem Cell* **9**, 588-598.

Chu, L.-T., Fong, S. H., Kondrychyn, I., Loh, S. L., Ye, Z. and Korzh, V. (2012). Yolk syncytial layer formation is a failure of cytokinesis mediated by Rock1 function in the early zebrafish embryo. *Biol. Open* **1**, 747-753.

Dekens, M. P. S., Pelegri, F. J., Maischein, H. M. and Nusslein-Volhard, C. (2003). The maternal-effect gene futile cycle is essential for pronuclear congression and mitotic spindle assembly in the zebrafish zygote. *Development* **130**, 3907-3916.

Dosch, R., Wagner, D. S., Mintzer, K. A., Runke, G., Wiemelt, A. P. and Mullins, M. C. (2004). Maternal control of vertebrate development before the midblastula transition: mutants from the zebrafish I. *Dev. Cell* **6**, 771-780.

Evsikov, S. V., Morozova, L. M. and Solomko, A. P. (1990). The role of the nucleocytoplasmic ratio in development regulation of the early mouse embryo. *Development* **109**, 323-328.

Evsikov, A. V., de Vries, W. N., Peaston, A. E., Radford, E. E., Fancher, K. S., Chen, F. H., Blake, J. A., Bult, C. J., Latham, K. E., Solter, D. et al. (2004). Systems biology of the 2-cell mouse embryo. *Cytogenet Genome Res.* **105**, 240-250.

Giraldez, A. J., Mishima, Y., Rihel, J., Grocock, R. J., Van Dongen, S., Inoue, K., Enright, A. J. and Schier, A. F., (2006). Zebrafish MiR-430 promotes deadenylation and clearance of maternal mRNAs. *Science* **312**, 75-79.

Hamatani, T., Carter, M. G., Sharov, A. A. and Ko, M. S. H. (2004). Dynamics of global gene expression changes during mouse preimplantation development. *Dev. Cell* **6**, 117-131.

Harvey, S. A., Sealy, I., Kettleborough, R., Fenyes, F., White, R., Stemple, D. and Smith, J. C. (2013). Identification of the zebrafish maternal and paternal transcriptomes. *Development* **140**, 2703-2710.

Heyn, P., Kircher, M., Dahl, A., Kelso, J., Tomancak, P., Kalinka, A. T. and Neugebauer, K. M. (2014). The earliest transcribed zygotic genes are short, newly evolved, and different across species. *Cell Rep.* **6**, 285-292.

Houwing, S., Berezikov, E. and Ketting, R. F. (2008). Zili is required for germ cell differentiation and meiosis in zebrafish. *EMBO J.* **27**, 2702-2711.

Hwang, S.-Y., Oh, B., Füchtbauer, A., Füchtbauer, E.-M., Johnson, K. R., Solter, D. and Knowles, B. B. (1997). Maid: a maternally transcribed novel gene encoding a potential negative regulator of bHLH proteins in the mouse egg and zygote. *Dev. Dyn.* **209**, 217-226.

Jevtić, P. and Levy, D. L. (2015). Nuclear size scaling during Xenopus early development contributes to midblastula transition timing. *Curr. Biol.* **25**, 45-52.

Jevtić, P. and Levy, D. L. (2017). Both nuclear size and DNA amount contribute to midblastula transition timing in Xenopus laevis. *Sci. Rep.* **7**, 7908.

Joseph, S. R., Pálfy, M., Hilbert, L., Kumar, M., Karschau, J., Zaburdaev, V., Shevchenko, A. and Vastenhouw, N. L. (2017). Competition between histone and transcription factor binding regulates the onset of transcription in zebrafish embryos. *Elife* **6**, e23326.

Kane, D. A. and Kimmel, C. B. (1993). The zebrafish midblastula transition. *Development* **119**, 447-456.

Kane, D. A., Hammerschmidt, M., Mullins, M. C., Maischein, H. M., Brand, M., van Eeden, F. J., Furutani-Seiki, M., Granato, M., Haffter, P., Heisenberg, C. P. et al. (1996). The zebrafish epiboly mutants. *Development* **123**, 47-55.

Kimmel, C. B. and Law, R. D. (1985). Cell lineage of zebrafish blastomeres. II. Formation of the yolk syncytial layer. *Dev. Biol.* **108**, 86-93.

Kimmel, C. B., Ballard, W. W., Kimmel, S. R., Ullmann, B. and Schilling, T. F. (1995). Stages of embryonic development of the zebrafish. *Dev. Dyn.* **203**, 253-310.

Korzh, V. (2009). Before maternal-zygotic transition. There was morphogenetic function of nuclei. *Zebrafish* **6**, 295-302.

Lee, M. T., Bonneau, A. R., Takacs, C. M., Bazzini, A. A., DiVito, K. R., Fleming, E. S. and Giraldez, A. J. (2013). Nanog, Pou5f1 and SoxB1 activate zygotic gene expression during the maternal-to-zygotic transition. *Nature* **503**, 360-364.

Lee, M. T., Bonneau, A. R. and Giraldez, A. J. (2014). Zygotic genome activation during the maternal-to-zygotic transition. *Annu. Rev. Cell Dev. Biol.* **30**, 581-613.

Lieberfarb, M. E., Chu, T., Wreden, C., Theurkauf, W., Gergen, J. P. and Strickland, S. (1996). Mutations that perturb poly(A)-dependent maternal mRNA activation block the initiation of development. *Development* **122**, 579-588.

Lindeman, L. C., Andersen, I. S., Reiner, A. H., Li, N., Aanes, H., Østrup, O., Winata, C., Mathavan, S., Müller, F., Alestrom, P. et al. (2011). Prepatterning of developmental gene expression by modified histones before zygotic genome activation. *Dev. Cell* **21**, 993-1004.

Marzluff, W. F. (2005). Metazoan replication-dependent histone mRNAs: a distinct set of RNA polymerase II transcripts. *Curr. Opin. Cell Biol.* **17**, 274-280.

Newport, J. and Kirschner, M. (1982). A major developmental transition in early Xenopus embryos: II. Control of the onset of transcription. *Cell* **30**, 687-696.

Obrig, T. G., Culp, W. J., McKeehan, W. L. and Hardesty, B. (1971). The mechanism by which cycloheximide and related glutarimide antibiotics inhibit peptide synthesis on reticulocyte ribosomes. *J. Biol. Chem.* **246**, 174-181.

Oh, B., Hwang, S., McLaughlin, J., Solter, D. and Knowles, B. B. (2000). Timely translation during the mouse oocyte-to-embryo transition. *Development* **127**, 3795-3803.

Onichtchouk, D., Geier, F., Polok, B., Messerschmidt, D. M., Mössner, R., Wendik, B., Song, S., Taylor, V., Timmer, J. and Driever, W. (2010). Zebrafish Pou5f1-dependent transcriptional networks in temporal control of early development. *Mol. Syst. Biol.* **6**, 354.

Pálfy, M., Joseph, S. R. and Vastenhouw, N. L. (2017). The timing of zygotic genome activation. *Curr. Opin. Genet. Dev.* **43**, 53-60.

Papapetrou, E. P., Tomishima, M. J., Chambers, S. M., Mica, Y., Reed, E., Menon, J., Tabar, V., Mo, Q., Studer, L. and Sadelain, M. (2009). Stoichiometric and temporal requirements of Oct4, Sox2, Klf4, and c-Myc expression for efficient human iPSC induction and differentiation. *Proc. Natl. Acad. Sci. USA* **106**, 12759-12764.

Pelegri, F. and Mullins, M. C. (2004). Genetic screens for maternal-effect mutations. *Methods Cell Biol.* **77**, 21-51.

Perez-Camps, M., Tian, J., Chng, S. C., Sem, K. P., Sudhaharan, T., Teh, C., Wachsmuth, M., Korzh, V., Ahmed, S. and Reversade, B. (2016). Quantitative imaging reveals real-time Pou5f3-Nanog complexes driving dorsoventral mesendoderm patterning in zebrafish. *Elife* **5**, e11475.

Piko, L. and Clegg, K. B. (1982). Quantitative changes in total RNA, total poly(A), and ribosomes in early mouse embryos. *Dev. Biol.* **89**, 362-378.

Potireddy, S., Vassena, R., Patel, B. G. and Latham, K. E. (2006). Analysis of polysomal mRNA populations of mouse oocytes and zygotes: dynamic changes in maternal mRNA utilization and function. *Dev. Biol.* **298**, 155-166.

Prioleau, M.-N., Huet, J., Sentenac, A. and Mechali, M. (1994). Competition between chromatin and transcription complex assembly regulates gene expression during early development. *Cell* **77**, 439-449.

Rizzino, A. (2013). Concise review: The Sox2-Oct4 connection: critical players in a much larger interdependent network integrated at multiple levels. *Stem Cells* **31**, 1033-1039.

Rott, N. N. and Sheveleva, G. A. (1968). Changes in the rate of cell divisions in the course of early development of diploid and haploid loach embryos. *J. Embryol. Exp. Morphol.* **20**, 141-150.

Salles, F. J., Darrow, A. L., O'Connell, M. L. and Strickland, S. (1992). Isolation of novel murine maternal mRNAs regulated by cytoplasmic polyadenylation. *Genes Dev.* **6**, 1202-1212.

Salles, F. J., Lieberfarb, M. E., Wreden, C., Gergen, J. P. and Strickland, S. (1994). Coordinate initiation of Drosophila development by regulated polyadenylation of maternal messenger RNAs. *Science* **266**, 1996-1999.

Sampath, P., Lee, Q. Y. and Tanavde, V. (2011). Identifying translationally regulated genes during stem cell differentiation. *Curr. Protoc. Stem Cell Biol.* 18:1B.8.1-1B.8.13.

Smedley, D., Haider, S., Ballester, B., Holland, R., London, D., Thorisson, G. and Kasprzyk, A. (2009). BioMart–biological queries made easy. *BMC Genomics* **10**, 22.
Solnica-Krezel, L. and Driever, W. (1994). Microtubule arrays of the zebrafish yolk cell: organization and function during epiboly. *Development* **120**, 2443-2455.
Subtelny, A. O., Eichhorn, S. W., Chen, G. R., Sive, H. and Bartel, D. P. (2014). Poly(A)-tail profiling reveals an embryonic switch in translational control. *Nature* **508**, 66-71.
Tadros, W. and Lipshitz, H. D. (2009). The maternal-to-zygotic transition: a play in two acts. *Development* **136**, 3033-3042.
Vastenhouw, N. L., Zhang, Y., Woods, I. G., Imam, F., Regev, A., Liu, X. S., Rinn, J. and Schier, A. F. (2010). Chromatin signature of embryonic pluripotency is established during genome activation. *Nature* **464**, 922-926.
Wagner, D. S., Dosch, R., Mintzer, K. A., Wiemelt, A. P. and Mullins, M. C. (2004). Maternal control of development at the midblastula transition and beyond: mutants from the zebrafish II. *Dev. Cell* **6**, 781-790.
Walser, C. B. and Lipshitz, H. D. (2011). Transcript clearance during the maternal-to-zygotic transition. *Curr. Opin. Genet. Dev.* **21**, 431-443.
Westerfield, M. (2000). *The Zebrafish Book. A Guide for the Laboratory Use of Zebrafish (Danio rerio)*. Eugene, Oregon: University of Oregon Press.
Winata, C. L., Kondrychyn, I., Kumar, V., Srinivasan, K. G., Orlov, Y., Ravishankar, A., Prabhakar, S., Stanton, L. W., Korzh, V. and Mathavan, S. (2013). Genome wide analysis reveals Zic3 interaction with distal regulatory elements of stage specific developmental genes in zebrafish. *PLoS Genet.* **9**, e1003852.
Xu, C., Fan, Z. P., Müller, P., Fogley, R., DiBiase, A., Trompouki, E., Unternaehrer, J., Xiong, F., Torregroza, I., Evans, T. et al. (2012). Nanog-like regulates endoderm formation through the Mxtx2-Nodal pathway. *Dev. Cell* **22**, 625-638.
Yabe, T., Ge, X. and Pelegri, F. (2007). The zebrafish maternal-effect gene cellular atoll encodes the centriolar component sas-6 and defects in its paternal function promote whole genome duplication. *Dev. Biol.* **312**, 44-60.
Yartseva, V. and Giraldez, A. J. (2015). The maternal-to-zygotic transition during vertebrate development: a model for reprogramming. *Curr. Top. Dev. Biol.* **113**, 191-232.
Zhao, B. S., Wang, X., Beadell, A. V., Lu, Z., Shi, H., Kuuspalu, A., Ho, R. K. and He, C. (2017). m6A-dependent maternal mRNA clearance facilitates zebrafish maternal-to-zygotic transition. *Nature* **542**, 475-478.

Supplementary Figure S1

Egg

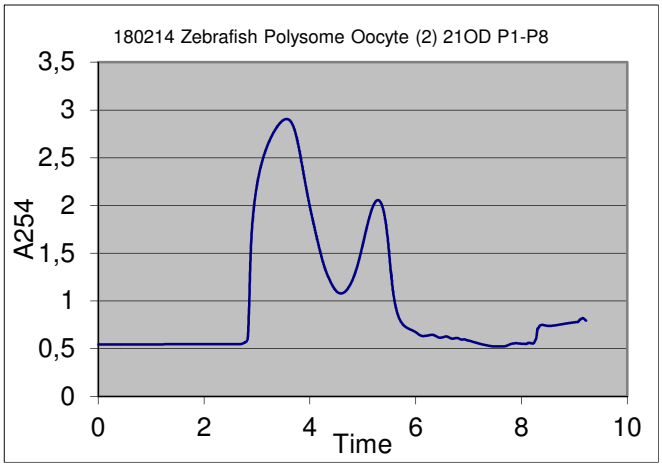

1-cell stage

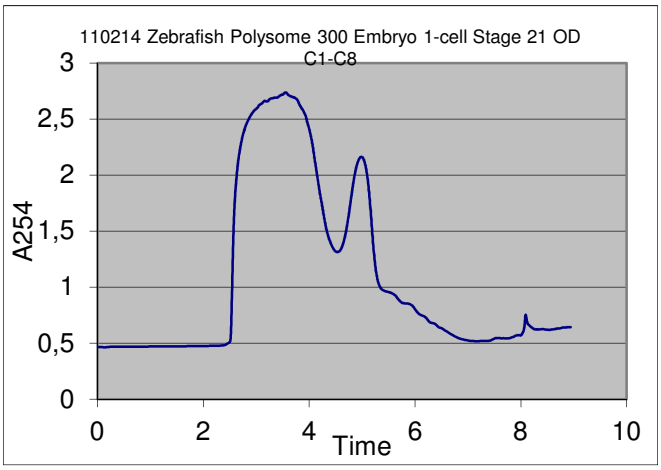

16-cell stage

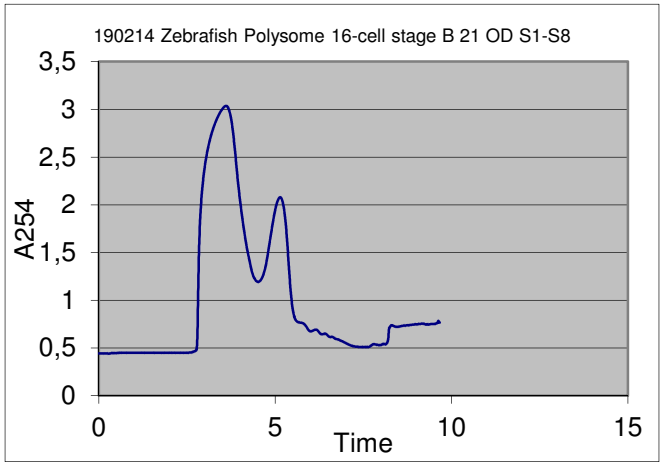

128-cell stage

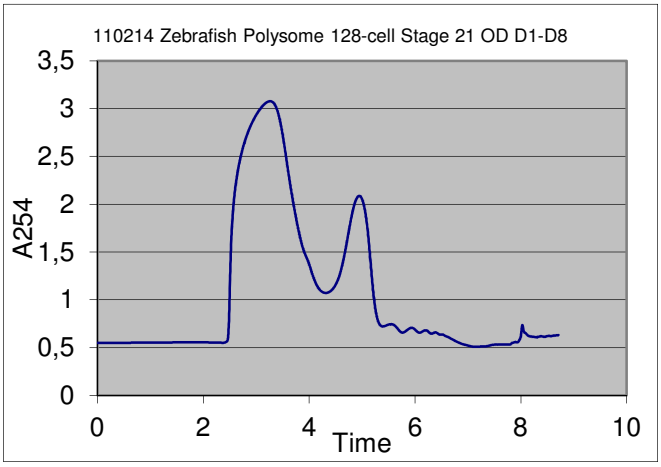

3.5hpf

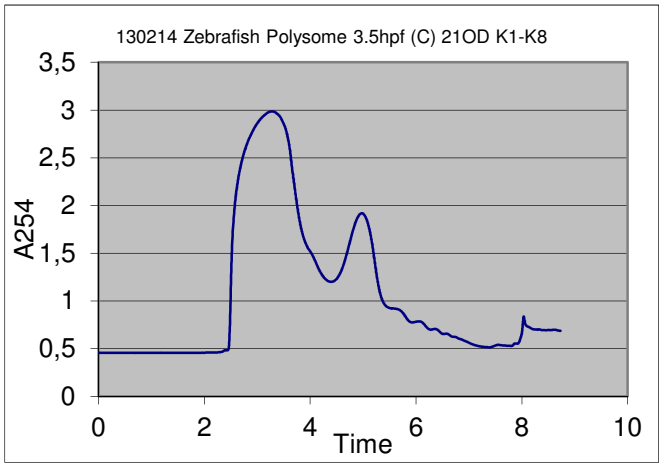

5.5hpf

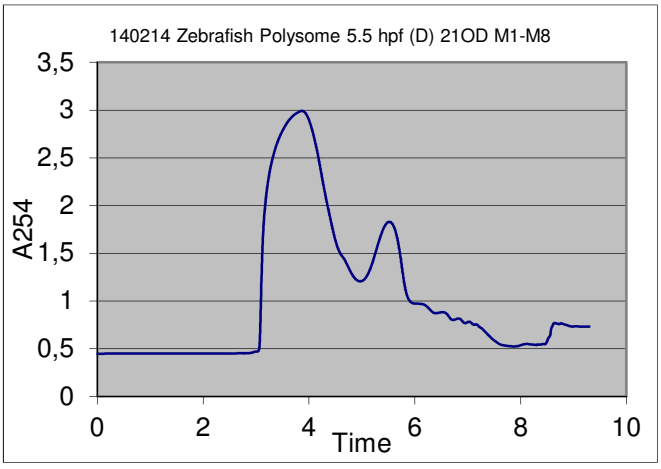

Supplementary Fig. S1. Polysome profile of early zebrafish embryos obtained by sucrose density gradient centrifugation.

Supplementary Figure S2

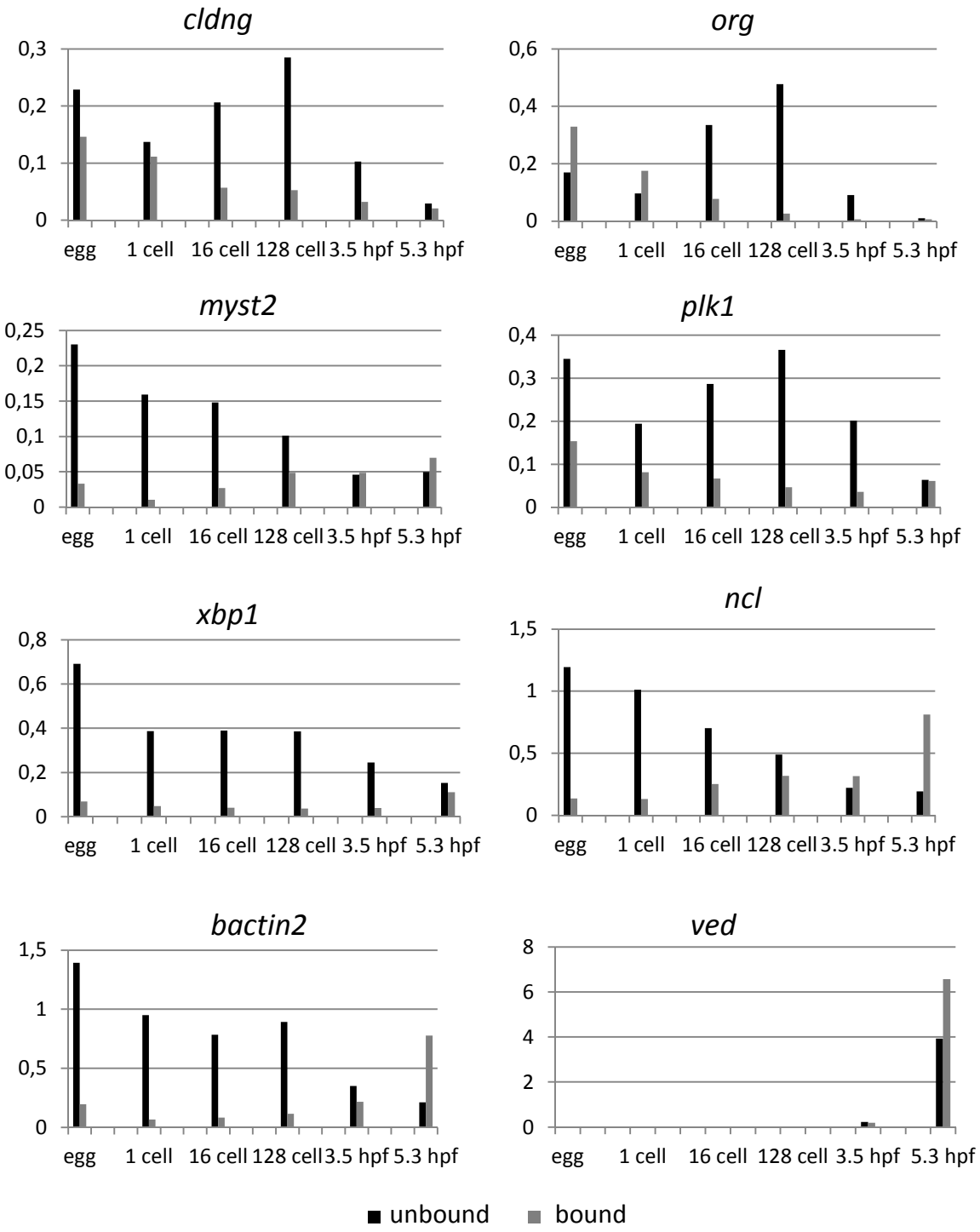

Supplementary Fig. S2. Real-time PCR validation of genes originating from different clusters (maternal non-CPA – *cldng, org, and plk1*; maternal CPA – *myst2, xbp1, ncl*, and *bactin2*; zygotic – *ved*) in polysome bound and unbound fractions.

Supplementary Figure S3

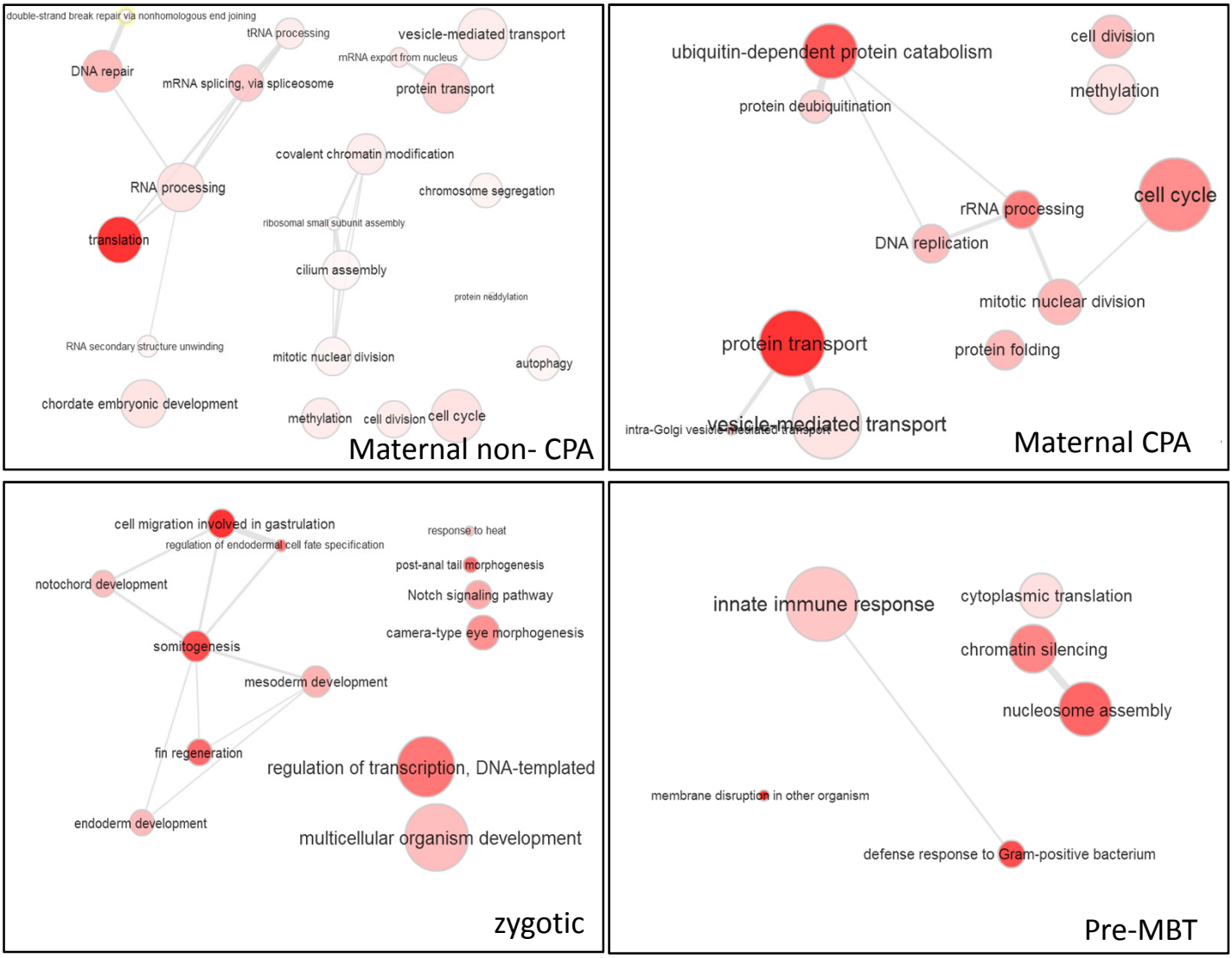

Supplementary Fig. S3. Network of significantly enriched (Benjamini-Hochberg p-value <=0.05) biological process terms in different expression clusters. Colour intensity represents higher significance for the particular term, while size of circle indicates relative number of genes within a group.

Supplementary Figure S4

Supplementary Fig. S4. Genome browser image showing an example of a novel transcribed region discovered in Chromosome 12 in 4 different samples (egg, polysome-unbound; 3.5 hpf, polysome-bound; 3.5 hpf, polysome-unbound, and 5.3 hpf, total). Protein domains enriched among the novel transfrags as revealed by Hmmr3 analysis.

Supplementary Figure S5

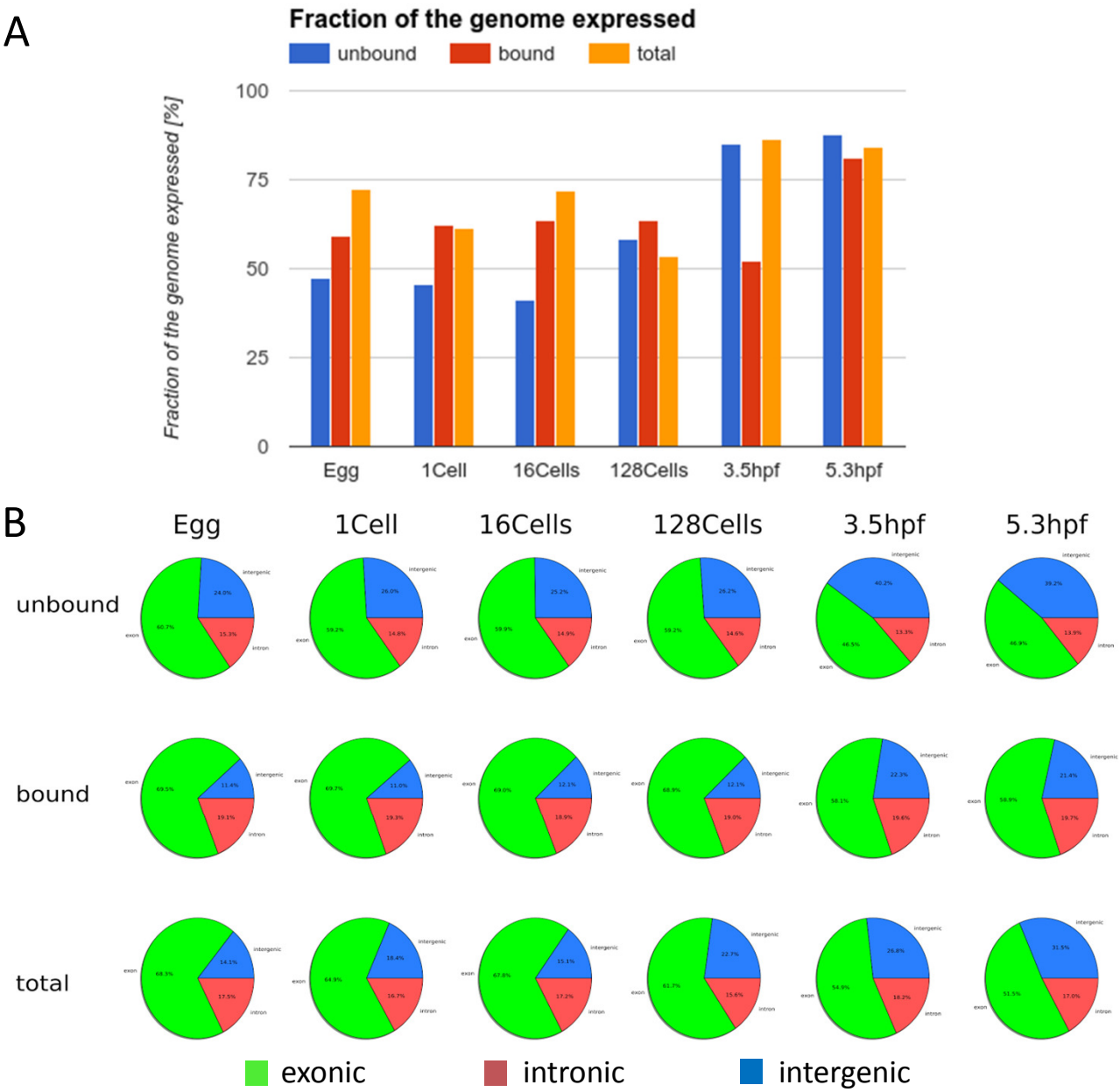

Supplementary Fig. S5. (A) Histogram shows the fraction of genome expressed represented by RNA-seq read coverage in total and polysome samples. (B) Pie charts representing the proportions of RNA seq reads mapping to different regions of the genome. Note the increase in intergenic mapping at MBT and post-MBT stage in all conditions.

Supplementary Figure S6

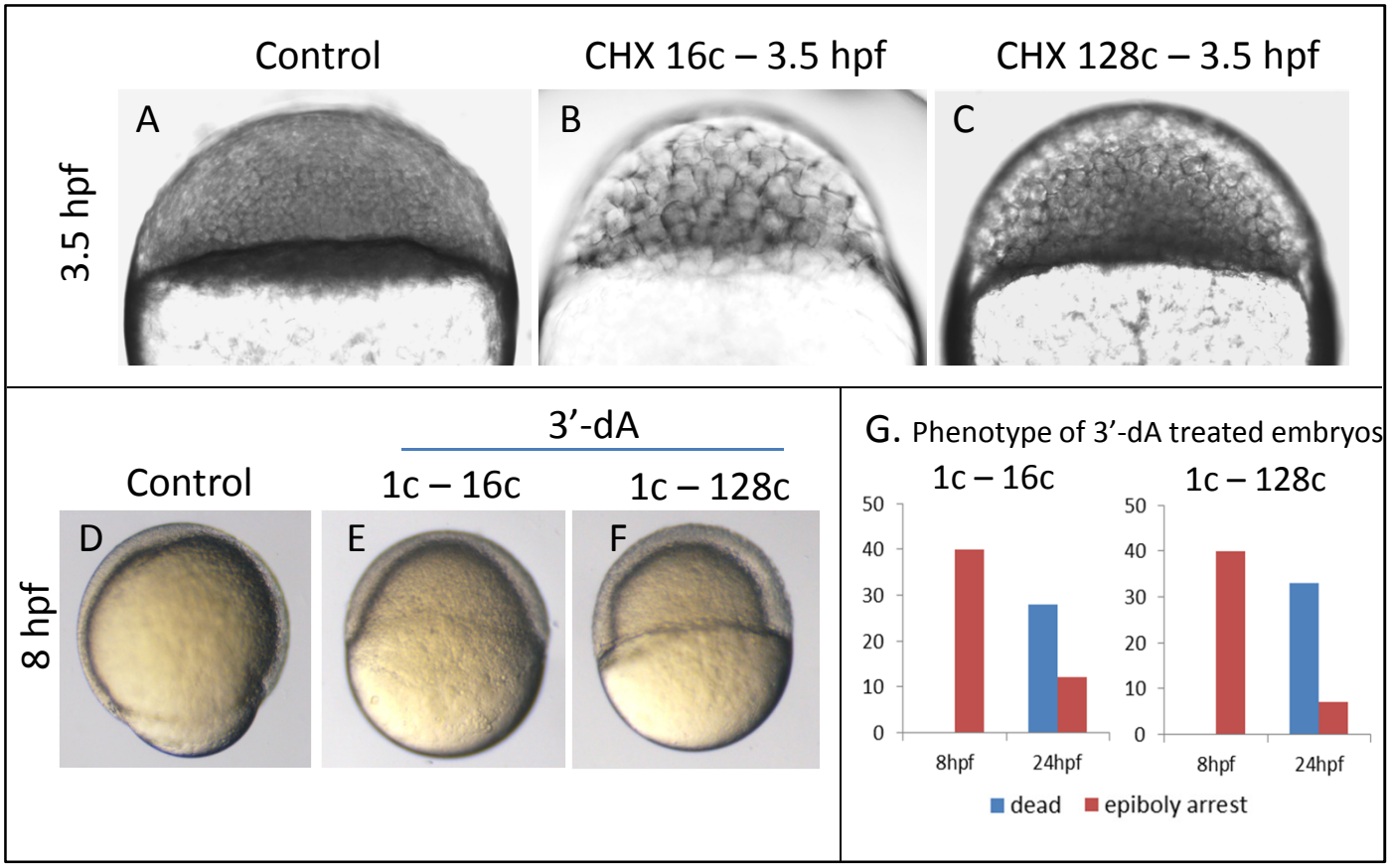

Supplementary Fig. S6. (A-C) Treatment of embryos with Cycloheximide (CHX) starting at different time points. Observation was done at 3.5 hpf. (D-F) Treatment of embryos with Cordycepin (3'-dA) starting from 1-cell stage and terminated at different stages prior to MBT. Observation was performed at 8 hpf. (G) Histogram showing the rate of epiboly arrest phenotype an mortality at 8 hpf and 24 hpf.

Bioinformatics analysis of RNA-seq data

Sequencing reads were mapped to the zebrafish Refseq genome assembly (GRCz10) using STAR v2.4.2a, ignoring non-canonical splice-sites. For polysome-bound, -unbound, and total unfractionated samples, raw read counts generated by Salmon 0.6.0 algorithm (Patro et al., 2017) were normalized according to library size. Normalization factors were calculated in R using DESeq2 method (Anders and Huber, 2010) across all samples. In order to eliminate low expressing transcripts, gene abundances within each fractionated library were represented in RPKM expression units, following which a cutoff of RPKM >= 1 was applied. Clustering was performed on total unfractionated samples and the poly(A)+ dataset from Aanes et al., (2011). Genes were assigned into 4 categories based on their expression dynamics: not expressed (mean expression less than 10 TPM), zygotic (mean expression prior to MBT < 10TPM and mean expression after MBT > 20TPM), pre-MBT (expression in 128-cell stage or earlier increases at least two-fold), and maternal. Calculations of transcriptional and translation rates were subsequently performed with the library size-normalized counts. Quality control of the sequencing libraries with FASTQC v0.11.3 revealed no clear association between quality measures and fraction of reads aligned from each library. All libraries except for the three best performing ones in terms of mapping rate contained overrepresented sequences which suggest the presence of adapters or PCR primers. To test how these sequences affect mapping, we plotted the fraction of reads containing adapters and PCR primers of each library to their mappability. Indeed, we observed an anticorrelation, which proved that both adapters and PCR primers make up the bulk of the unmappable reads (Pearson r = -0.887). Nevertheless, overall mapping of the sequencing reads was high, ranging from 72.02% to 90.81% for uniquely mapped reads. For hierarchical clustering, the transcript level abundance and count estimates from Salmon algorithm were summarized to gene-level and imported to DESeq2

using tximport 1.0.2 (Soneson et al., 2015). The regularized log transformation from the DESeq2 package was used on the data and the sample-to-sample distances were plotted with pheatmap package.

We interrogated the distribution of mapped sequencing reads throughout the whole genome. In the case of egg and pre-MBT stages, the transcriptome is assumed to consist entirely of maternally deposited mRNAs, therefore the genomic coverage of the reads represent the fraction of maternal genome which is transcribed and deposited to the embryo to control pre-zygotic development leading to MBT. We considered introns in between a pair of exon-spanning reads as being transcribed although it is spliced out in the mature mRNA. Taking into account only base-pair positions covered by three or more reads in total unfractionated mRNA, an average of 64.76% of the maternal genome is represented by the egg and pre-MBT (1-cell, 16-cell, and 128-cell) total transcriptome (Suppl. Fig. S3A). Based on our experiment, it is not possible to distinguish between residual maternal mRNAs and newly transcribed zygotic mRNAs in the MBT and post-MBT stages. Nevertheless, a significant increase in genomic representation could be observed in these stages (85.4% on average). In general, polysome-unbound fractions represented a lower percentage of the maternal genome in egg and all pre-MBT stages unlike that in MBT and post-MBT stages.

We then calculated the number of reads aligned to different types of genomic regions and classified them into genic (exonic and intronic) and intergenic regions. Distinct distribution patterns of reads mapping to these different regions could be observed in different samples (Suppl. Fig. S3B). Similarly, clear differences were observed between pre- and post-MBT stages with intergenic regions more enriched in post-MBT stages. Higher percentage of exonic regions was present in polysome-bound fraction at all stages compared to the

polysome-unbound fraction. This was expected since mostly coding regions are translated. However the presence of intronic regions as well as intergenic regions in this fraction suggests the presence of previously unidentified gene regions or alternatively spliced exons. It is unlikely that these are immature mRNAs as maternal mRNAs are known to be provided as fully spliced forms. Interestingly, the proportion of intergenic regions increased about twofold at MBT (3.5 hpf) and post-MBT (5.3 hpf) in all fractions, including polysome-bound fractions (Suppl. Fig. S3B). One possibility is that these are immature mRNAs from new zygotic transcription at MBT. However, the proportion of introns did not increase at MBT onwards, suggesting that it is unlikely that immature mRNAs contribute to the sequenced pool of transcripts. Alternatively, these may represent novel unannotated transcripts, noncoding RNAs, or expressed genomic regulatory regions. With the knowledge that enhancers and other genomic elements could produce transcripts, it is not unreasonable to expect that these may be present in the RNA-seq data.

Testing of differential distribution between maternal CPA and non-CPA subclusters was performed by applying the Wilcoxon-Mann-Whitney two-sample rank-sum test for either ΔTL or ΔTS between maternal CPA and non-CPA subclusters with the alternative hypothesis: true shift is not equal to 0. Each comparison yielded significant p-value ($p<2.2e-16$ for all ΔTL comparisons; $p<0.01$ for all ΔTS comparisons). Estimator of pseudomedian is plotted in Fig. 2H-I with error bars representing 95% confidence interval in the median dynamics plot.

Gene Ontology (GO) was performed using the Database for Annotation, Visualization, and Integrated Discovery (DAVID; Huang et al., 2009) and Metascape (http://metascape.org ; Tripathi et al., 2015) and visualized using REViGO (Supek et al., 2011) tools. Biological

pathway network analyses was performed using Metascape with integrated Cytoscape tool for visualization of network.

The reads from Harvey (Harvey et al., 2013) dataset were re-aligned onto GRCz10 assembly using BWA MEM v0.7.12 and STAR v020201 for exome and transcritome, respectively. Subsequently, both lines (SATf-WIKm, WIKf-SATm) were genotyped using samtools mpileup v0.1.19 with parameters -I -q 15 -Q 20. Sites that differ between mother and father, 163,829 in total, were used to quantify the frequency of father-specific allele in all samples. Subsequently, each allele has been assigned to respective gene. We defined paternal genes (4,169) as those that exhibit at least 10% of father-specific allele in RNA-seq reads across 5.3 hpf samples. In contrast, maternal genes (487) are those having father-specific allele frequency below 10% in 5.3 hpf samples.

Discovery of novel transcripts

In order to identify novel transcripts, we aligned RNA-seq reads using GSNAP version 2015-12-31 and STAR 2.4.2a and compared the performance between the two splice-aware short sequence aligners. GSNAP was found to produce on average 3% more uniquely aligned reads (up to 10% more for alignments above mapping quality 0). Cufflinks also reported 7% more multi-exon transcripts assembled using GSNAP alignments compared to that from STAR. Symmetric difference between transcripts assembled on STAR and GSNAP alignments showed more annotated transcripts present in the GSNAP subgroup. Based on these observations, GSNAP was chosen for downstream novel transcripts analysis. The reads were trimmed using cutadapt 1.9.1 (e=<0.1; q>=20; O>3; m>=20, trimming universal Illumina TruSeq adapter sequence AGATCGGAAGAGC). Reads were subsequently aligned with GSNAP aligner onto the *Danio rerio* GRCz10 reference genome assembly (filter chastity =

both; max-mismatches=5; batch=5; use-shared-memory=1; novel splicing =1; force-single-end). Using these parameters, on average 87.57% of all reads were uniquely aligned across all samples. Transcriptome assembly was subsequently performed using Cufflinks 2.2.1 with Ensembl release 83 genome annotation. Cuffcompare was run to compare and annotate the newly assembled transcripts. On average, 64.25% of transcripts were multi-exonic, 39.34% of total transcripts had FPKM > 5 and 14.37% of total transcripts had multiple exons and FPKM > 5. Novel transcripts were extracted from the cuffcompare tracking file and statistics were gathered using custom python script. Potential coding regions were identified using TransDecoder (Haas et al., 2013), which identifies transcripts with open reading frames of at least 100 amino acids long. Additionally, coding transcript retention was enhanced using BLAST protein sequence search on Uniref90 protein database and Pfam search using HMMER v3.1b2 to identify common protein domains. The BLAST expectation value threshold was set as TransDecoder suggested value 1e-5. The HMMER E-value was left as the default 10. Transdecoder evaluated coding transcripts were extracted from the original cufflinks transcript.gtf files for each sample separately. Next, the extracted annotation files were combined using cuffcompare. Expression values were aggregated for each novel super-locus per sample as well as for each novel transfrag per sample. 1080 non-overlapping gene models were obtained with ORFs on the correct strand corresponding to the RNA-seq reads.

Clones used for Whole mount in situ hybridization

Partial cDNA clone for *camsap2a2* were amplified using the following primer pairs: forward 5′-CGCAGAGCCTGTTGAGAATCC-3′ and reverse 5′-GATGAGTCCTCGTCGAGTGTC-3′ and cloned into the pGEM-TEasy vector (Promega). Partial cDNA clone of *wnt8a* (CK709337.1) was obtained from the GIS collection. pBluescript goosecoid was a gift from John Postlethwait (Addgene plasmid #16935; Thisse et al., 1994).

References

Anders, S., Huber, W., 2010. Differential expression analysis for sequence count data. Genome biology 11, R106.

Haas, B.J., Papanicolaou, A., Yassour, M., Grabherr, M., Blood, P.D., Bowden, J., Couger, M.B., Eccles, D., Li, B., Lieber, M., Macmanes, M.D., Ott, M., Orvis, J., Pochet, N., Strozzi, F., Weeks, N., Westerman, R., William, T., Dewey, C.N., Henschel, R., Leduc, R.D., Friedman, N., Regev, A., 2013. De novo transcript sequence reconstruction from RNA-seq using the Trinity platform for reference generation and analysis. Nature protocols 8, 1494-1512.

Harvey, S.A., Sealy, I., Kettleborough, R., Fenyes, F., White, R., Stemple, D., Smith, J.C., 2013. Identification of the zebrafish maternal and paternal transcriptomes. Development 140, 2703-2710.

Patro, R., Duggal, G., Love, M.I., Irizarry, R.A., Kingsford, C., 2017. Salmon provides fast and bias-aware quantification of transcript expression. Nat Methods 14, 417-419.

Soneson, C., Love, M.I., Robinson, M.D., 2015. Differential analyses for RNA-seq: transcript-level estimates improve gene-level inferences. F1000Research 4, 1521.

Supek F, Bošnjak M, Škunca N, Šmuc T., 2011. REVIGO summarizes and visualizes long lists of Gene Ontology terms. PLoS ONE. doi:10.1371/journal.pone.0021800.

Huang da W, Sherman BT, Lempicki RA, 2009. Systematic and integrative analysis of large gene lists using DAVID bioinformatics resources. Nat Protoc 4: 44–57.

Thisse C, Thisse B, Halpern ME, Postlethwait JH, 1994. Goosecoid expression in neuroectoderm is disrupted in zebrafish cyclops gastrulas. Dev Biol 164(2): 420-9.

Tripathi S, Pohl MO, Zhou Y, Rodriguez-Frandsen A, Wang G, Stein DA et al., 2015. Meta- and Orthogonal Integration of Influenza "OMICs" Data Defines a Role for UBR4 in Virus Budding. Cell Host & Microbe, 18: 723-735.

Supplementary Tables

Supplementary Table_S1 – Mapping details of RNA-seq samples

Click here to Download Table S1

Supplementary Table_S2 – List of genes in each expression clusters

Click here to Download Table S2

Supplementary Table_S3 - GO (Biological Process) enrichment of maternal nonCPA cluster

Click here to Download Table S3

Supplementary Table_S4 - GO (Biological Process) enrichment of maternal CPA cluster

Click here to Download Table S4

Supplementary Table_S5 - GO (Biological Process) enrichment of zygotic cluster

Click here to Download Table S5

Supplementary Table_S6 - GO (Biological Process) enrichment of preMBT cluster

Click here to Download Table S6

Supplementary Table_S7 – Calculations of transcriptional and translational rates

Click here to Download Table S7

Supplementary Table_S8 – List of microarray differentially expressed genes in 3'd(A) treatment. Click here to Download Table S8

Supplementary Table_S9- GO (Biological Process) enrichment of microarray downregulated genes

Click here to Download Table S9

Supplementary Table_S10 - GO (Biological Process) enrichment of microarray upregulated genes

Click here to Download Table S10

Supplementary Table_S11 – List of 3'd(A) upregulated genes which are targets of Ythdf2 and miR-430.

Click here to Download Table S11

Supplementary Table_S12 - GO (Biological Process) enrichment of microarray downregulated zygotic genes

Click here to Download Table S12

Supplementary Table_S13 - GO (Biological Process) enrichment of microarray downregulated preMBT genes

Click here to Download Table S13

Supplementary Table_S14 - GO (Biological Process) enrichment of microarray upregulated maternal nonCPA genes

Click here to Download Table S14

Supplementary Table_S15 - GO (Biological Process) enrichment of microarray upregulated maternal CPA genes

Click here to Download Table S15

Supplementary Table_S16 – Annotation of novel transcribed regions (BLAST and Pfam)

Click here to Download Table S16

Supplementary Table_S17 – Genomic coordinates of novel transcribed regions

Click here to Download Table S17

Supplementary Table_S18 – List of genes in common with other datasets

Click here to Download Table S18